



# Development of a 2-km resolution ocean model covering the coastal seas around Japan for operational application

Kei Sakamoto<sup>1</sup> · Hiroyuki Tsujino<sup>1</sup> · Hideyuki Nakano<sup>1</sup> · Shogo Urakawa<sup>1</sup> · Takahiro Toyoda<sup>1</sup> · Nariaki Hirose<sup>1</sup> · Norihisa Usui<sup>1</sup> · Goro Yamanaka<sup>1</sup>

Received: 30 January 2019 / Accepted: 17 July 2019 / Published online: 20 August 2019  
© Springer-Verlag GmbH Germany, part of Springer Nature 2019

## Abstract

In order to expand the coastal ocean monitoring and forecasting system of the Japan Meteorological Agency from the Seto Inland Sea to the entire coastal seas of Japan, a 2-km resolution model has been newly developed. We investigated the model performance based on a 4-year hindcast experiment without data assimilation. The model realistically reproduced basic distributions and seasonal variations of sea surface temperature, salinity, sea level, etc. Small-scale features in the coastal seas, such as fronts, were also well simulated due to the high resolution. Daily sea level variations on the coasts followed the tide gauge observation with an error of 7.1 cm on average. Transports through main Japanese straits were also consistent with previous research. In addition to expanding the domain, some dynamical elements are newly introduced. One of the major updates is implementing of explicit tides with high precision, as the amplitude error was only 9.2% and the phase error was 10.2° for the M2 tide. The second is coupling of a sea ice model reproducing the seasonal development of sea ice in the Sea of Okhotsk. The third is introduction of approximately 4000 river inflows across Japan to improve salinity in coastal seas. Introduction of the inverse barometer effect and high-resolution atmospheric forcings also contributed to coastal sea level variations. The Japan Meteorological Agency plans to widely utilize the model with a new data assimilation system for coastal disaster prevention and oceanic condition monitoring, and our verification results support the utility of the model.

**Keywords** Coastal modeling · Japanese coastal seas · Operational model · Tides · Coastal front

## 1 Introduction

The Japan Meteorological Agency (JMA) has been conducting monitoring and forecasting of the western North Pacific Ocean mainly focusing on seas around Japan since 2001 and has provided the information widely to society. The current operational system is an ocean model and data assimilation system developed at the Meteorological Research Institute (MRI), MOVE/MRI.COM-WNP. This system reproduces the western boundary currents and offshore mesoscale eddies with a horizontal resolution of approximately 10 km

and forecasts for 30 days. In 2016, in order to respond to social needs for information about coastal disaster prevention and oceanic conditions, JMA also began operation of a system downscaling from MOVE/MRI.COM-WNP to the Seto Inland Sea, which is the largest inland sea of Japan. This new system, MOVE/MRI.COM-Seto, uses a numerical model with a resolution of approximately 2 km, which is 5 times finer, and adopts a new data assimilation method called incremental 4D-VAR (Usui et al. 2015). Using the new system, JMA monitors and forecasts for 11 days oceanic conditions such as temperature, salinity, currents, and sea levels in the Seto Inland Sea every day. (details of the Seto Inland Sea model are described in Sakamoto et al. (2016), which was published in the first issue of COSS-TT (Mey et al. 2017). Following the success of MOVE/MRI.COM-Seto, JMA is currently planning a next-generation system that extends the downscaling domain to the entire coastal seas of Japan. We have developed a new ocean model, MRI.COM-JPN, as its foundation.

Many ocean models with a horizontal resolution of approximately 10 km, called eddy resolving models, have

Responsible Editor: Guillaume Charria

This article is part of the Topical Collection on *Coastal Ocean Forecasting Science supported by the GODAE OceanView Coastal Oceans and Shelf Seas Task Team (COSS-TT) - Part II*

✉ Kei Sakamoto  
ksakamot@mri-jma.go.jp

<sup>1</sup> Meteorological Research Institute, Nagamine, Tsukuba, Ibaraki 305-0052, Japan

been developed for the western North Pacific Ocean including Japan. Although there remain challenges such as tuning to reproduce the Kuroshio path, a model design has been roughly established by many studies. Several long-term reanalysis datasets using data assimilation have also been created and widely used as a basis for ocean research around Japan (Usui et al. 2017; Miyazawa et al. 2017; Kuroda et al. 2017). On the other hand, models covering the entire coastal seas of Japan with a sub-mesoscale resolution of a few kilometers (here called a high-resolution Japanese coastal model) are under development, and most of them have been used for process studies. For example, Sakamoto et al. (2010) examined the dynamics of the coastal Oyashio Current by a 2-km resolution western North Pacific model (based on MRI.COM). Urakawa et al. (2015) studied formation of low-salinity plumes of river water origin by a 2-km resolution Japanese coastal model (COCO). Varlamov et al. (2015) examined excitation of M2 internal tides by a 3-km resolution Japanese coastal model named JCOPE-T (POM). Uchiyama et al. (2017) investigated relations between eddies of the Kuroshio region and primary production by a 3-km resolution Japanese coastal model (ROMS) coupled a NPZD model under climatology forcings. Though high-resolution Japanese coastal models expressing various coastal processes are under development, as the JCOPE-T model started operation in 2018, there are no models widely tested for reproducibility yet. Development of such a model is still a challenge for coastal ocean modeling.

In developing the new model, MRI.COM-JPN, we decided to base on the Seto Inland Sea model already in operation in order to alleviate the difficulty. In particular, the horizontal resolution is the same 2 km (strictly  $1/33^\circ \times 1/50^\circ$ ). Also commonly, the model is designed to be a versatile model that incorporates as many physical elements as possible, which will be used as a general-purpose platform of the JMA's coastal marine operations in the future. Meanwhile, with the advent of progress in ocean modeling, we incorporated some new functions. Major improvements include coupling a sea ice model, introducing explicit tides, introducing depression and suction of the sea surface by atmospheric pressure (the inverse barometer effect), and increasing the resolution of river runoff data. In addition, we upgraded the downscaling method to a double two-way nesting method coupling with a global model and a North Pacific model. Besides them, we have also made various improvements as explained in Section 2.

Although it is an upgrade of the Seto Inland Sea model, there were several challenges in development of MRI.COM-JPN. First, since the model domain expands to a vast area from the tropical Kuroshio upper region to the subarctic Okhotsk Sea, it is necessary to reproduce more diverse coastal processes. It must reproduce the branching of the Kuroshio current to the Tsushima Warm Current in the

East China Sea, southward transport of the sea ice by the East Sakhalin Current, and so on. Second, in order to incorporate a sea ice model and a tide scheme without reducing the whole reproducibility of the model, their many control parameters should be tuned carefully. Third, the change from one-way nesting to two-way nesting made the model control more difficult, together with the expansion of the model domain. For the Seto Inland Sea model, the domain was small, and the model could be controlled by the lateral boundaries. However for MRI.COM-JPN, we have to control each of the global, basin, and coastal models by model dynamics. In this regard, we could make use of the knowledge about global and basin models developed at MRI (Nakano et al. 2013; Urakawa et al. 2019). Furthermore, it was also a difficult subject that numerical costs increased dramatically since the domain was expanded 21 times from the Seto Inland Sea model. As explained in Section 2, we have devoted much effort to computational efficiency. For data assimilation, various advances were also required from MOVE/MRI.COM-Seto. For interested readers, see Hirose et al. (2019).

In this paper, we investigate the model performance from various viewpoints, based on a 4-year hindcast experiment driven by atmospheric reanalysis data. In order to focus on the performance of the model itself, we use mainly results of so-called free-run experiments where initialization by data assimilation was not used. Focusing on technical model setup and overall verification, the paper is organized as follows. First, we describe detailed specifications of the model and settings of the hindcast experiment (Section 2). Next, we examine reproducibility about oceanic conditions of the entire model domain (Section 3.1), temperature and salinity fields, and currents in coastal regions (Sections 3.2 and 3.3). In addition, sea level variations at Japanese coasts are systematically examined on a wide time scale (Section 4). Finally, the model validations and the future issues are summarized (Section 5).

## 2 Model and experimental design

### 2.1 Model configurations

Configurations of MRI.COM-JPN are summarized in Table 1. The OGCM used is the Meteorological Research Institute Community Ocean Model Ver.4.5 (MRI.COM; Tsujino et al. 2017). The MRI.COM is a depth coordinate model that solves the primitive equations under the hydrostatic and Boussinesq approximations. The model adopts an Arakawa B-grid arrangement (1972), and coastlines are created by connecting tracer points instead of velocity points (Fig. 1a). Since it is possible to make straits with a width of one grid cell, this grid arrangement is suited

**Table 1** Main settings of MRI.COM-JPN. Items with \* are the same as the Seto Inland Sea model (Sakamoto et al. 2016)

Numerical model	MRI.COM Ver.4.5
Coordinates	Free-surface $z^*$ coordinate (vertical) and polar coordinate (horizontal)
Region	117–160° E, 20–52° N
Horizontal resolution*	$1/33^\circ \times 1/50^\circ$ (approximately 2 km)
Vertical resolution	2–700 m (60 levels) (minimum water depth of 8 m)
Grid size	$1423 \times 1604 \times 60 = 136,949,520$
Tracer advection	SOM (Prather 1986) with a flux limiter (Merryfield and Holloway 2003)
Horizontal viscosity	Smagorinsky-like biharmonic (Griffies and Hallberg 2000) with additional harmonic viscosity near the lateral boundaries
Horizontal diffusion	Biharmonic (diffusivity = $1 \times 10^{15} \text{ cm}^4 \text{ s}^{-1}$ )
Vertical turbulent mixing	GLS scheme (Umlauf and Burchard 2003) using the default coefficients of MRI.COM (Sec. 15.4 of Tsujino et al. 2017)
Downscaling	Two-way on-line double-nesting method
Sea ice	5-category sea ice model (Mellor and Kantha 1989; Hunke and Dukowicz 1997, 2002)
Tides	Main 8 tidal constituents (Sakamoto et al. 2013)
Inverse barometer effect	Explicitly considered
Surface boundary	Wind, pressure: MSM data, radiation, precipitation, temperature, dew point temperature: JRA55do ver.1.3 data. The bulk formula of Large and Yeager (2004) and the solar altitude scheme of Ishizaki and Yamanaka (2010) are used. The relative wind effect factor $\alpha$ is 0.15
River runoff	JRA55do + a hourly dataset based on the JMA's river runoff index
Relaxation condition	Sea surface salinity is restored to monthly climatology with a piston velocity of 2 m per 14.6 days, and raised sharply when it falls below 10.
Time step interval	3 min for baroclinic component, 7.5 s for barotropic component

for modeling of Japanese coastal seas, where the topography is complicated, as explained in Sakamoto et al. (2016). We adopted the  $z^*$  vertical coordinate system (Fig. 1b). As a result, the constraint of the minimum water depth of 32 m in the Seto Inland Sea model was relaxed to 8 m, and the expression of shallow coastal topography improved. See Appendix A of Sakamoto et al. (2016) for its effect. Bottom slopes are represented smoothly by a partial cell technique. See the MRI.COM manual (Tsujino et al. 2017) for the details of the model framework.

The model MRI.COM-JPN is a double-nested model that couples three models: a global one (called the GLB model), a North Pacific one (NP model), and a Japanese coastal one (JPN model). The JPN model domain is the entire coastal seas of Japan, spanning from 117 to 160° E and from 20 to 52° N (Fig. 2). All the lands of Japan are included in the model domain. The horizontal resolution is  $1/33^\circ$  in the zonal direction and  $1/50^\circ$  in the meridional direction, corresponding to approximately 2 km. This resolution is the same as the preceding Seto Inland Sea model and is

**Fig. 1** a Horizontal and b vertical grid arrangements of the MRI.COM. Temperature, salinity, and SSH are defined at the circle, while velocity and the water depth are defined at the crosses. The vertical coordinate is basically a depth coordinate (broken lines in b), but the sea level deviation (thick line) is distributed to each layer through the water column (solid line) (so-called  $z^*$  coordinates)

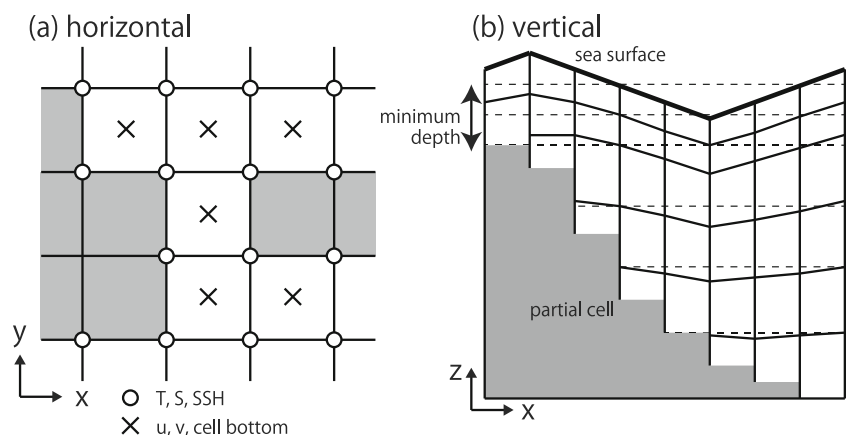
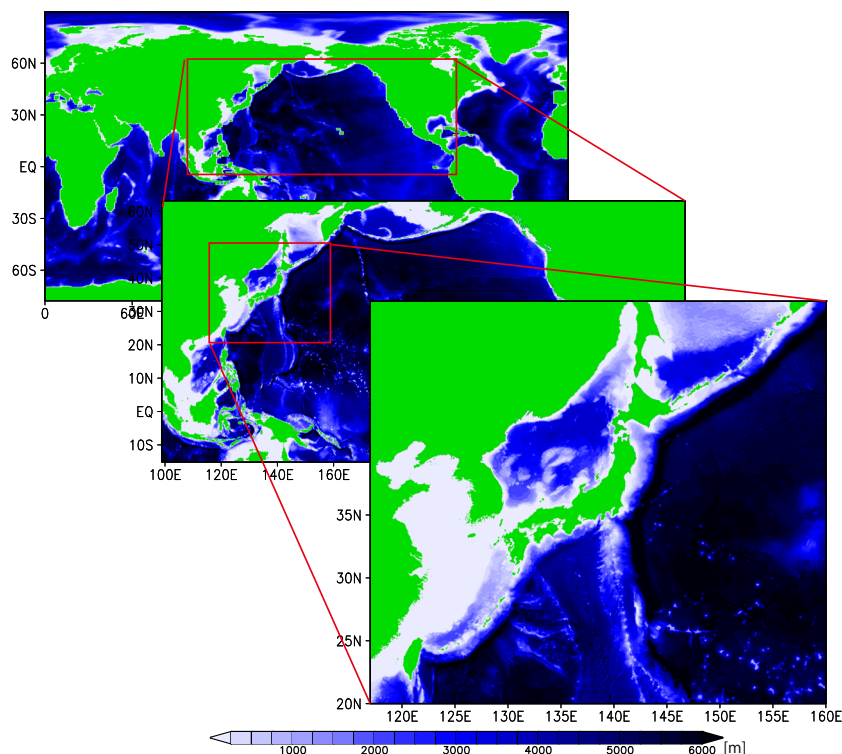


**Fig. 2** The model regions and the bathymetry of the MRI.COM-JPN three models



necessary to represent major coastal topographies of Japan. The model has 60 levels in the vertical direction with thickness increasing from 2 m at the surface to 600 m at 6300-m depth. The model grid size is  $1423 \times 1604 \times 60$ , i.e. approximately 137 million. The bathymetry is based on the JTOPO30v2 dataset, though some parts are modified to represent coast lines realistically. The GLB model covers the entire world oceans with horizontal resolution of  $1^\circ \times 0.5^\circ$ , and the NP model covers the North Pacific Ocean spanning from  $99^\circ \text{ E}$  to  $80^\circ \text{ W}$  and from  $15^\circ \text{ S}$  to  $63^\circ \text{ N}$  with horizontal resolution of  $1/11^\circ \times 1/10^\circ$ . Both the GLB model and the NP model have the same 60 levels as JPN.

We adopted model schemes suitable for small-scale phenomena in the same manner as the Seto Inland Sea model, with some additional improvements. The tracer advection is the same high-precision second-order moment scheme (Prather 1986), but the flux limiter of Merryfield and Holloway (2003) is introduced to further suppress overshoot and undershoot. The horizontal viscosity is a biharmonic friction with a Smagorinsky-like viscosity (Griffies and Hallberg 2000), while the horizontal diffusion is a biharmonic type with a constant diffusivity ( $1 \times 10^{15} \text{ cm}^4 \text{ s}^{-1}$ ). We changed the vertical turbulent mixing scheme from Noh and Kim (1999) to the GLS scheme (Umlauf and Burchard 2003) in order to represent more realistically coastal bottom mixing by tidal currents. For the background vertical diffusivity, a three-dimensional field tuned for model stability was used.

The model implemented some new processes which were not considered in the Seto Inland Sea model. First, we introduced the main 8 tidal constituents using our tide scheme (Sakamoto et al. 2013). Since this scheme adopts an approach to calculate the temporal evolution of the tides by their own governing equations, we can incorporate tide-specific effects such as self-attraction and loading (the SAL effect). Utilizing this advantage, we introduced tides with high precision in a wide area as shown in Section 4.2, by tuning various tidal parameters (specifically, 0.88 for the SAL coefficient,  $400 \text{ m}^2 \text{ s}^{-1}$  for the horizontal viscosity of the tidal currents, 0.0025 for the bottom friction coefficient, and so on). The second is the inverse barometer effect, i.e. suction and depression of the sea surface by atmospheric pressure. The model is expected to be utilized for coastal disaster prevention, so this effect is explicitly incorporated to the model through the pressure gradient in the barotropic equation, in order to reproduce sea level rise events such as storm surge (an example of the results will be shown in Section 4.4). A sea ice model is also newly incorporated, since the Okhotsk Sea and the northern part of the Sea of Japan, where the sea ice is formed in winter, are included in the model domain. The sea ice model used is a 5-category model, where the sea ice is classified according to sea ice thickness. Their thermodynamics are based on the work by Mellor and Kantha (1989), and dynamics are based on an elastic-viscous-plastic rheology of Hunke and Dukowicz (1997, 2002).

A two-way on-line double-nesting method is used for downscaling. The lateral boundaries of the JPN model are given from the NP model, and the lateral boundaries of the NP model are from the GLB model for each time step. On the other hand, the physical quantities calculated in the JPN model and the NP model are reflected to the NP model and the GLB model, respectively, for each time step. In this way, the three models run synchronously at the same time step interval while communicating mutually. As a result, compared with a one-way nesting method adopted by the Seto Inland Sea model, the model variables of the parent models and the child models are more smoothly connected at the lateral boundaries so that numerical instability at the boundaries is suppressed (Debreu and Blayo 2008; Debreu et al. 2012). It is also an important feature that the volume is preserved in the whole models. As an example, time variations of the water volumes in the oceans and the sea ice and snow are shown in Fig. 3 for the model experiment described in Section 2.2. In the experiment, the water volume of the sea ice and snow increased from January to June (winter in the Southern Hemisphere), while that in the oceans decreased. However, there was no change in the sum of both, meaning that the water volume in the 3-model system was preserved. This preservation is expected to be usable for research on long-term coastal sea level variations accompanied by climate change.

Two sets of data were mixed and used for atmospheric forcings. For radiation, precipitation, atmospheric temperature, and dew point temperature on the sea surface, we

used the dataset of JRA55-do ver.1.3, a forcing dataset for long-term driving of an ocean model based on the JRA-55 long-term reanalysis (Tsujino et al. 2018). This dataset provides 3-h data with horizontal resolution of 55 km. For wind and atmospheric pressure around Japan, we used the MSM reanalysis dataset created by JMA, which is a 1-h reanalysis of a mesoscale model with horizontal resolution of approximately 5 km. In general, it is better to avoid mixing two datasets in terms of the consistency of the calculated sea surface fluxes, but within the scope of this model experiment, the combination of the two was the best for reproducibility. The high-spatiotemporal resolution wind and pressure of MSM clearly contributed to the reproducibility of coastal sea level variations, that is one of the main targets of the model (Section 3.3). On the other hand, by using radiation and precipitation of JRA55-do carefully corrected for driving ocean models, sea surface temperature and salinity were maintained in a realistic range even in long-term free-run experiments. In fact, we also conducted experiments using radiation and precipitation of MSM, but coastal sea surface temperature and salinity were largely drifted (not shown). The surface fluxes were computed based on these datasets and the bulk formulas of Large and Yeager (2004). Daily variations of solar altitude were also taken into account by the scheme of Ishizaki and Yamanaka (2010). It should be noted that wind stress vector  $\tau$  is computed by using the wind vector of the surface air  $u_a$ , the first level velocity (surface current)  $u_s$ , and a bulk transfer coefficient  $C_D$  as follows:

$$\tau = \rho_a C_D |u_a - \alpha u_s| (u_a - \alpha u_s), \tag{1}$$

where  $\rho_a$  is the density and  $\alpha$  is the contribution of the surface current to the calculation of relative surface wind, i.e. the relative wind effect factor (Sec. 14.1.1 of Tsujino et al. 2017). It has been pointed out that around 0.7 is recommended for  $\alpha$  because of the “current feedback” effect that approximately 30% of the ocean current velocity is reflected to ocean surface wind speed (Renault et al. 2019a, b). However, within the scope of this model experiment, priority is given to the reproducibility of the results, and values of 0.15 in the JPN model and 0.02 in the NP model were adopted from several case studies. Dependence on  $\alpha$  will be discussed in Section 3.1 Regarding river runoff, it is important to use as high-resolution data as possible, since its impact on coastal seas is large. We created hourly runoff data of 3986 rivers across Japan based on the JMA runoff index, which is a land surface model output for flood forecast (Urakawa et al. 2016). For rivers other than around Japan, 1/4° resolution data provided by JRA55-do was used.

The boundary conditions of the topography have not changed from the Seto Inland Sea model. The boundary

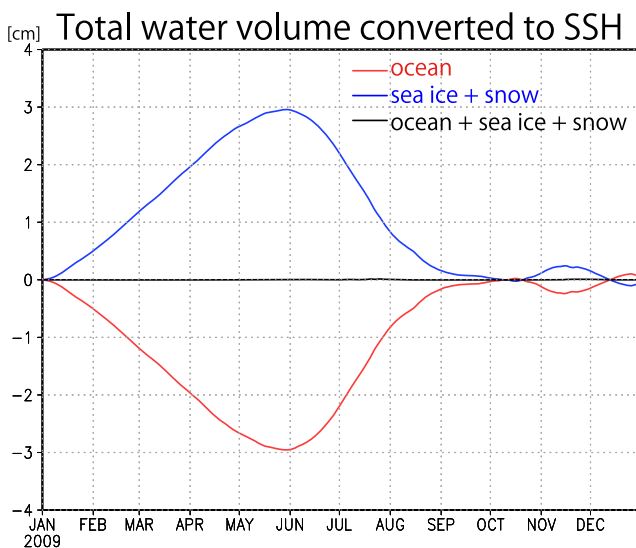


**Fig. 3** Time series of the ocean water volume integrated in the 3-model system (blue), the water volume contained in the sea ice and snow (red), and the sum of both (black) for 1 year. The results of the control experiment are shown. The values are the deviation from January converted into the global average sea level

conditions for momentum are a quadratic friction with a coefficient of  $1.25 \times 10^{-3}$  at the bottom and a no-slip condition at the lateral boundaries of the bottom topography. No tracer flux is imposed at both of the boundaries. The NP model and the GLB model basically use specifications of a North Pacific model (Nakano et al. 2013; Usui et al. 2017) and a global model (Yukimoto et al. 2019; Urakawa et al. 2019), respectively, which have been developed at MRI. Their details are omitted here.

Since the model will be used operationally, we also tried to improve numerical stability as follows. (1) Numerical instability was likely to occur at some coastal topographies around Japan. They were modified. (2) Although excitation of disturbances at the lateral boundaries was suppressed to some extent by two-way nesting, the model tended to be unstable near the boundaries. We tried to stabilize nesting according to Chapter 18 of Tsujino et al. (2017). Specifically, in the buffer zones adjacent to the boundaries, a Laplacian horizontal viscosity was added, and the deviation from the value of the parent model was smoothed. Furthermore, the background vertical viscosity was increased at a part of the northern boundary. (3) We used a stabilization option of MRI.COM which solves vertical advection implicitly when vertical velocity approaches the CFL condition. (4) We restored sea surface salinity (SSS) to a monthly climatology with a piston velocity of 2 m per 14.6 days. (5) When SSS falls below 10, it is raised immediately to 10 (while preserving the whole salt amount of the model). This is to prevent salinity from becoming negative in undershoot by the advection scheme. Since salinity of river inflow is prescribed as zero and inflow of each river is given by only one grid on the coast, negative salinity may occur after large flooding without this measure. With these measures, the model ran stably with the time step interval of 3 min for the baroclinic component and 7.5 s for the barotropic component, using a mode-splitting technique.

We have also worked on computational efficiency for a long time, such as introduction of OpenMP, utilization of SIMD parallelization, omitting of land nodes in two-dimensional MPI parallelization, and bulk MPI communication of multiple variables in order to reduce the frequency of node communication. Especially, in a large-scale two-way nesting, a lot of communication is required between models. Thus, by using a coupler named S-Cup, which has been developed at MRI (Yoshimura and Yukimoto 2008), many-to-many inter-node communication is performed to speed up the model. In addition, in feedback from the child models to the parent models, we devised measures to reduce data communication, such as omitting communications unrelated to the time evolution of the model. By working on these, the computational time was shortened to less than half from the beginning of the model

development so that it took only 18 days to integrate the model for 4 years by 48 nodes of Fujitsu FX100.

## 2.2 Experimental design

To validate the model performance, a control experiment was executed by the following procedure. We started the experiment by using a data assimilation experiment result of December 2, 2008, as the initial value (Hirose et al. 2019), and ran the model until December 31, 2012, using the MSM and JRA55-do forcings as explained in Section 2.1. The experiment results for 4 years from 2009 to 2012 were used for analysis. To focus on characteristics and performance of the model itself, we included no initialization or correction by data assimilation (a so-called “free-run” experiment).

In the analysis, the results of the above control experiment are shown unless otherwise noted. In order to investigate the influence of the resolution, results of an experiment running only the GLB and NP models are also used in Section 3.2.

The following observational datasets were used for the validation:

- MODIS satellite SST data provided by Japan Aerospace eXploration Agency and the Tokai University (2009–2012).<sup>1</sup> The data were used after quality control based on the gridded SST dataset of JMA (MGDSST). The horizontal resolution is  $1/100^\circ$ .
- AVISO satellite sea level altitude data (2010).<sup>2</sup> The horizontal resolution is  $0.25^\circ$ .
- JMA coastal tide gauge observation (2009–2012). It covers the coasts across Japan by approximately 200 sites. Hourly data and daily mean data are used.
- JMA 5-daily analysis of the sea ice concentration (February 2011).
- Monthly mean sea surface salinity acquired from the Seto Inland Sea Comprehensive Water Quality Survey (2009).<sup>3</sup>

Generally speaking, observational data are not sufficient in coastal seas of Japan as stated in Sakamoto et al. (2016). In particular, there are few data which can be directly compared with internal structures of temperature, salinity, and currents in the model results. In this paper, we use mainly satellite and coastal tide gauge observations, which are provided continuously, although information is limited to the sea surface. Verification of the internal structure was only compared with figures of several papers (Han et al. 2016; Yu et al. 2016).

<sup>1</sup>[http://kuroshio.eorc.jaxa.jp/ADEOS/mod\\_nrt/](http://kuroshio.eorc.jaxa.jp/ADEOS/mod_nrt/)

<sup>2</sup><https://www.aviso.altimetry.fr/en/home.html>

<sup>3</sup><http://www.pa.cgr.mlit.go.jp/chiki/suishitu/index.html>

### 3 Results: oceanic conditions

#### 3.1 Overview

Before showing detailed verification in coastal seas, we show the basic reproducibility of the whole model domain such as water mass distributions and their seasonal variations. Figure 4 is the monthly mean sea surface temperature (SST) in February and August 2009. The overall distribution in the model was similar to the satellite observation in both February and August. In February (Fig. 4a), the warm water carried by the Kuroshio current was distributed from east of Taiwan to south of Japan and in the Kuroshio Extension region. Meanwhile, the cold water carried by the Oyashio current was distributed from east of the Kuril Islands to southeast of the Hokkaido Island. There was a transition region between the two water masses, forming a complex front structure. In the Sea of Japan, warm water was seen along with the Tsushima Warm Current from west of the Honshu Island to west of the Sakhalin Island.

A realistic temperature distribution was also obtained in August, which means that basic seasonal variations were reproduced (Fig. 4c). Characteristics in coastal areas, such as cooling along the Kuril Islands, were also reproduced. Root mean square error (RMSE) against the monthly SST satellite data was 1.31 °C on average for 2009–2012. (RMSE in February and August 2009 shown in Fig. 4 were nearly average values as 1.42 °C and 1.06 °C, respectively.) In addition, the region averaged temperature was 0.3 °C lower in summer and 0.4 °C higher in winter than the satellite data, which means that seasonal variations were slightly underestimated. For comparison, RMSE was evaluated about the model results of Sakamoto et al. (2010), whose data were only available among the past high-resolution Japanese coastal models listed in Section 1. As a result, RMSE was up to 2.10 °C. The bias of the region averaged temperature was also large, as it was 1 °C lower in summer and 1 °C higher in winter. Since their experiment used atmospheric forcings with no inter-annual variation (so-called normal year forcings), all these improvements

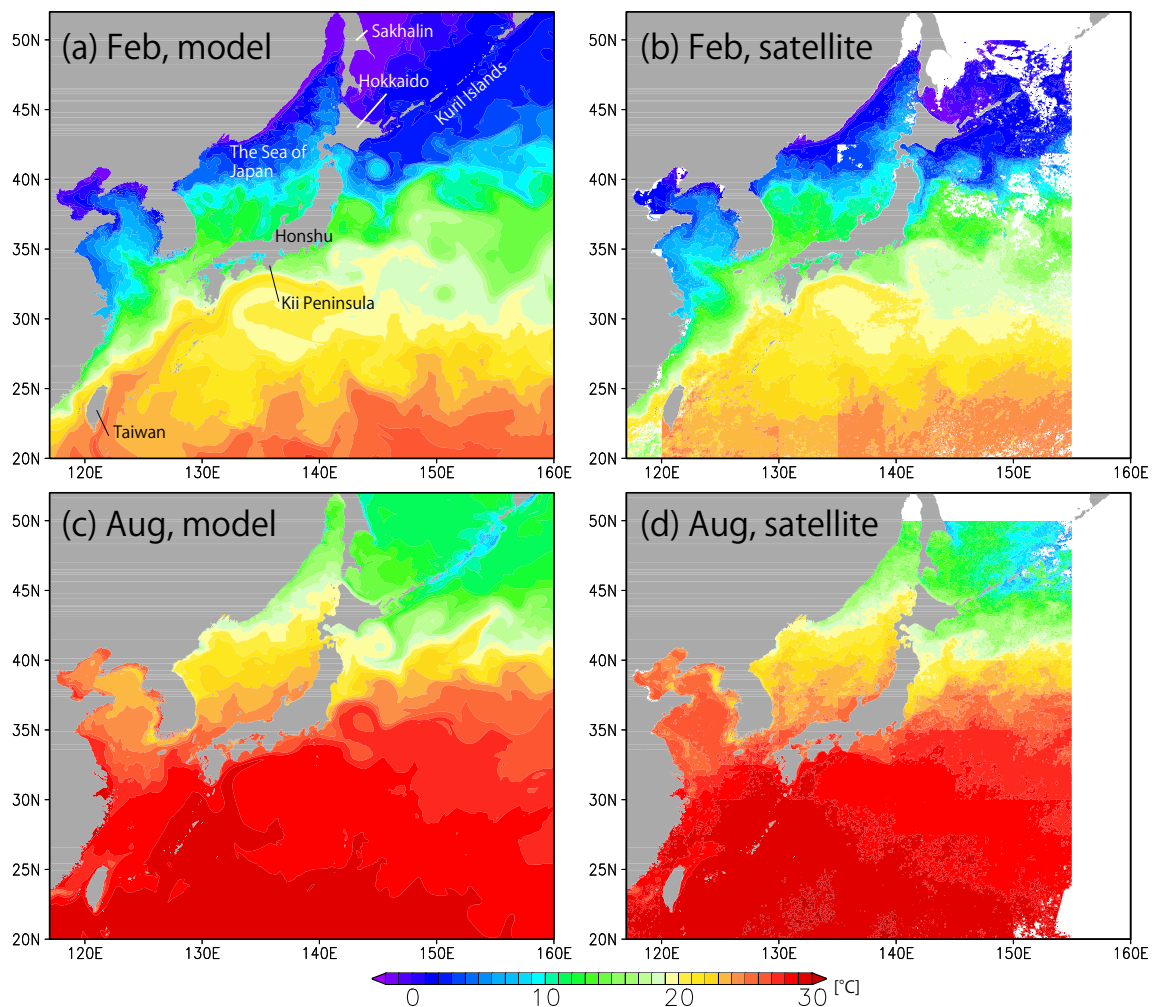
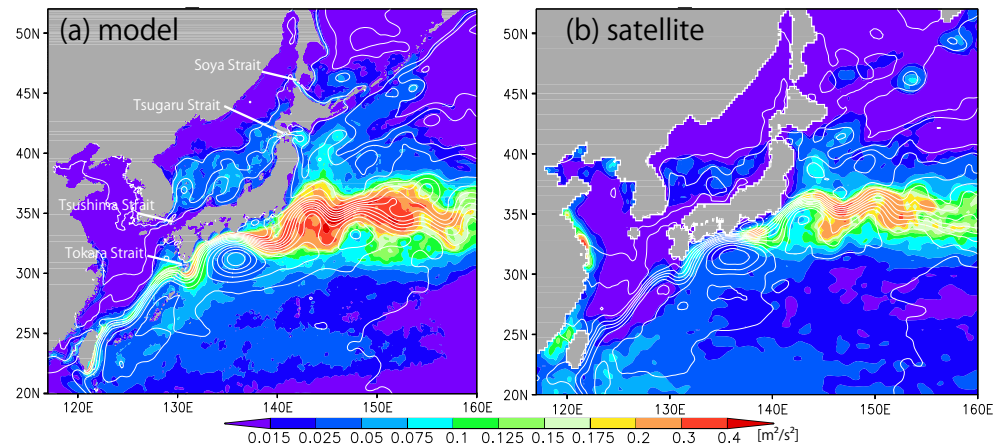


**Fig. 4** Monthly mean SST in February and August 2009 for **a, c** the model and **b, d** the satellite observation

**Fig. 5** Sea surface geostrophic eddy kinetic energy  $EKE_g$  (color shade) and the mean sea level (white line) in 2009–2012 for **a** model and **b** satellite altimetry data AVISO. The contour interval of the mean sea level is 10 cm



in reproducibility cannot be attributed to the model improvements. Nevertheless, as a model system including atmospheric forcing data, the fact that the RMSE decreased by 38% shows a clear improvement in reproducibility. Although not shown, sea surface salinity was consistent with available observation data (e.g. Japan Oceanographic Data Center archive). For example, the low-salinity water due to runoff of the Changjiang River (the Changjiang diluted water) reached Japan through the Tsushima Strait in summer, as suggested by Senjyu et al. (2006).

The sea surface height (SSH) distribution shown in Fig. 5 also corresponded well to the observation. A sharp SSH gradient accompanied by the Kuroshio current was formed south of Japan, as indicated in the SST distribution. A recirculation eddy was seen in the vicinity of 136° E, similar to the observation, though it was slightly stronger in the model. It is also realistic that the contour lines diverged in the Kuroshio Extension region east of 140° E. In the Sea of Japan, a contour line extended from the Tsushima Strait to the Tsugaru Strait and the Soya Strait while meandering, as seen in the observation.

The color shade in Fig. 5 shows the eddy kinetic energy of the sea surface geostrophic currents,  $EKE_g$ , calculated

from the daily mean sea level minus tides and barometric response,  $\eta_g$ , by

$$u_g = -\frac{g}{f} \frac{\partial \eta_g}{\partial y}$$

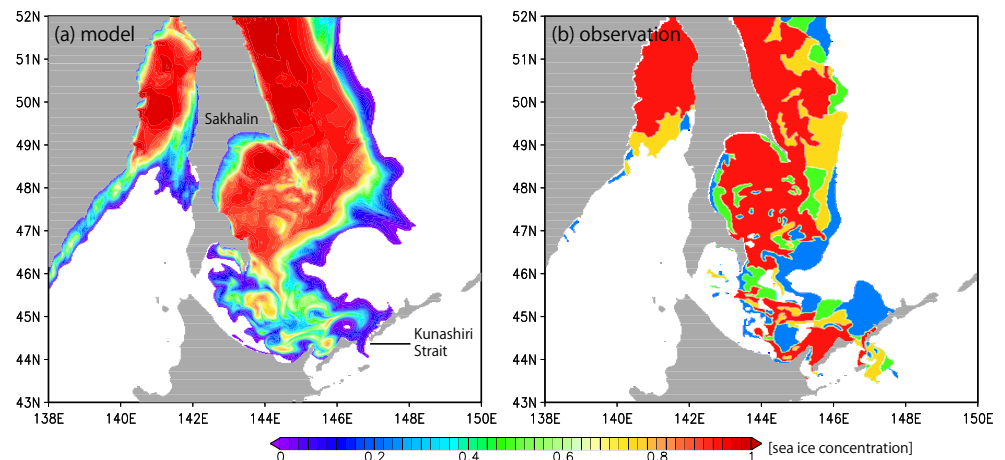
$$v_g = \frac{g}{f} \frac{\partial \eta_g}{\partial x}$$

$$EKE_g = \frac{1}{2} \overline{(u_g - \bar{u}_g)^2 + (v_g - \bar{v}_g)^2}$$

$$= \frac{g^2}{2f^2} \left\{ \overline{\left( \frac{\partial(\eta_g - \bar{\eta}_g)}{\partial x} \right)^2} + \overline{\left( \frac{\partial(\eta_g - \bar{\eta}_g)}{\partial y} \right)^2} \right\} \quad (2)$$

where the overbars indicate the annual mean,  $g$  is the gravitational acceleration,  $f$  is the Coriolis parameter, and  $(u_g, v_g)$  is the sea surface geostrophic current vector. Comparison with  $EKE_g$  calculated from the AVISO data shows that it was realistically reproduced, as well as SSH. This indicates that the fluctuation of the Kuroshio current and the mesoscale eddy activity were reasonable in the model. However,  $EKE_g$  was somewhat larger in the model, which may be caused by factors filtered out in the low-resolution AVISO data such as internal tides and sub-mesoscale variations. The value of  $EKE_g$  in the model

**Fig. 6** Sea ice concentration for **a** the model and **b** the observation on February 10, 2011





depended on the relative wind effect factor  $\alpha$  modulating wind stress by Eq. 1. When  $\alpha$  was close to 1,  $EKE_g$  decreased and the Kuroshio tended to flow offshore from the Tokara Straits, while when it was 0,  $EKE_g$  became excessive. Based on several case studies, this model uses a value of 0.15. We also tried tuning to add a horizontal viscosity of the Laplacian type for the control of the eddy activity, but it was not adopted in this model since the fluctuation of the Kuroshio current became excessive despite the decline of  $EKE_g$ .

At the end of this section, the reproducibility of the sea ice distribution is shown. The Sea of Okhotsk is the main region where the sea ice appears around Japan. Also in the model, the sea ice was transported southward by the East Sakhalin Current in winter. In the sea ice distribution on February 10, 2011 (Fig. 6), the sea ice arrived at the east end of the Hokkaido Island and flowed out through the Kunashiri Strait to the Pacific, similar to the observation. A filament structure was seen at the southern part of the Sea of Okhotsk, and coastal polynies were found along east coasts of the Sakhalin Island. These features are also consistent. To our knowledge, few studies have verified model simulations of the sea ice in the Sea of Okhotsk (Watanabe et al. 2004; Fujisaki et al. 2007, 2010), and it is a notable achievement that the seasonal development of the sea ice was well simulated by the high-resolution model.

### 3.2 Temperature and salinity in coastal regions

Next, some model results in coastal regions are shown. As a representative example, Fig. 7 shows a SST distribution south of the Hokkaido Island. In this region, the cold Oyashio water below 2 °C, the warm Kuroshio water above 8 °C, and the Tsugaru Warm Current water with intermediate temperature collide, leading to complex structures in SST. In the model, sharp and fine frontal structures among the water masses were simulated owing to the high resolution (Fig. 7a). For example, a wave structure of tens of kilometers was seen on the offshore front of the Tsugaru Warm Current, which was very similar to the satellite observation (Fig. 7b). In the open sea east of 143° E, there was a warm water eddy that has been cut off from the Kuroshio current. Although such stochastic phenomena cannot be directly compared with observations in free-run experiments, sharp fronts, filaments, and eddy structures formed between the eddy and the northern Oyashio water also appeared in the model. On the other hand, in the 10-km resolution model, the basic distribution of the water masses was the same but no complicated structure was seen on the fronts (Fig. 7c).

In order to more clearly show the difference in the SST front structure due to the model resolution, the absolute horizontal gradient  $|\nabla_h T|$  is shown in Fig. 8, where  $T$  is

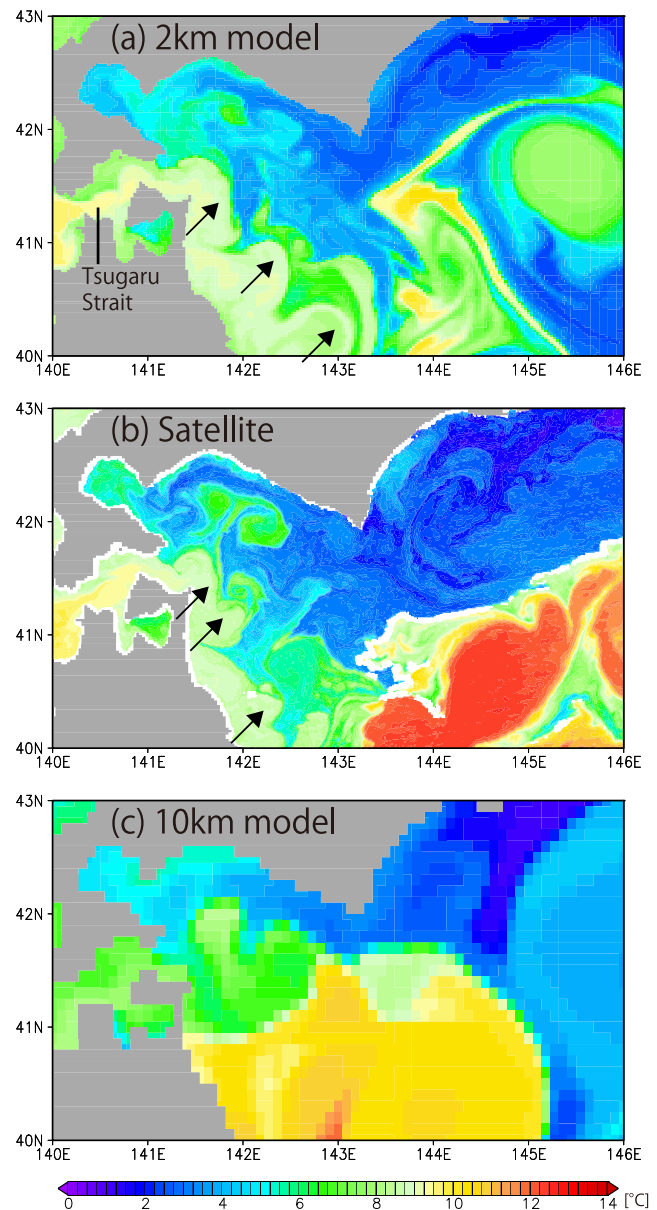


**Fig. 7** SST south of the Hokkaido Island on April 7, 2009, for **a** the model (the control experiment), **b** the satellite observation, and **c** the 10-km resolution model. The arrows in **a** and **b** show a wave structure on the offshore front of the Tsugaru Warm Current

SST and  $\nabla_h$  is the horizontal differential operator. In the control experiment, narrow bands with the SST gradient of  $1.5 \times 10^{-5} \text{ }^\circ\text{C cm}^{-1}$ , that is  $1.5 \text{ }^\circ\text{C km}^{-1}$ , appeared along the boundaries of the water masses. Such sharp temperature fronts are very similar to the result of the satellite observation. In the 10-km resolution model, frontal structures were simple and the SST gradient was as small as  $0.5 \text{ }^\circ\text{C km}^{-1}$  at the most (Fig. 8c). In this way, simulation of coastal phenomena remarkably improved due to the high resolution. However, it must be noted that the structures seen at the satellite observation (resolution 1 km) could not

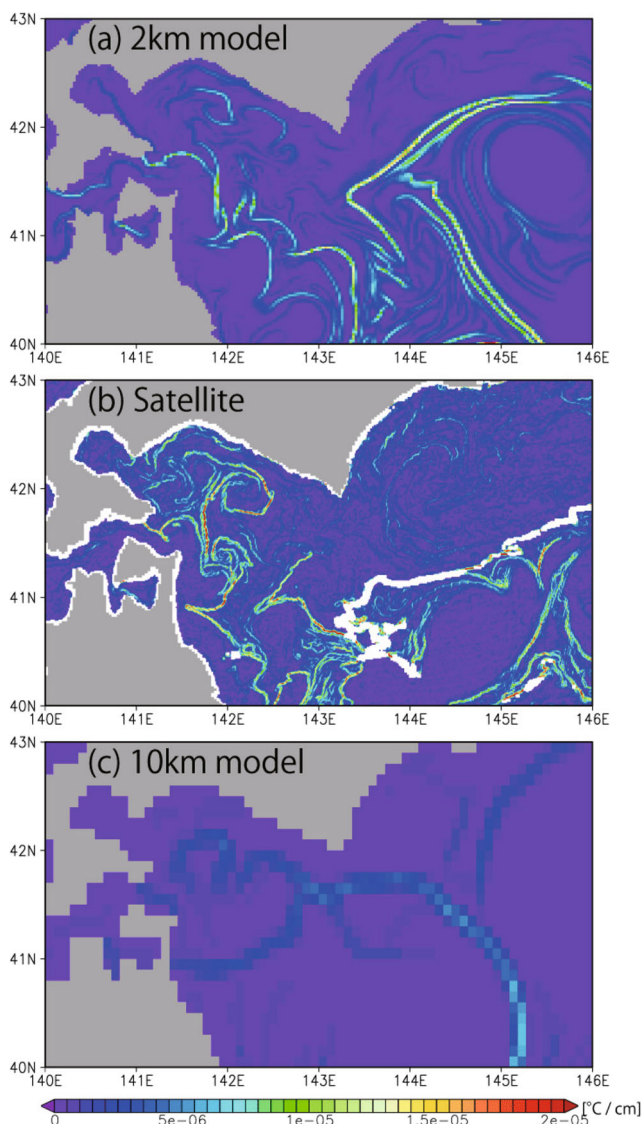


**Fig. 8** The magnitude of the horizontal gradient of SST,  $|\nabla_h T|$ . Others are the same as Fig. 7

be simulated sufficiently even at the horizontal resolution of 2 km, as seen from comparison between the model (Fig. 8a) and the satellite observation (Fig. 8b). Here, the region south of the Hokkaido Island, where the water masses collide, is shown as a representative example, but fronts having such a small structure are ubiquitous in the coastal seas of Japan, such as the Kuroshio front south of the Shikoku Island shown in Sakamoto et al. (2016).

The tides introduced to the model also contributed to the reproducibility of coastal SST. As an example, we focus on SST of the Bungo Channel in summer (Fig. 9). In the model results, a cold zone below 24 °C appeared inside the channel, with which a front with a temperature difference of approximately 4 °C was formed on the south side. This feature is in good agreement with the satellite observation,

suggesting that formation of a so-called tidal front was reproduced. The tidal front is a SST front formed between an open ocean and a coastal region where stratification is broken by vigorous bottom mixing due to strong tides (Simpson and Hunter 1974; Yanagi and Koike 1987).

In order to confirm that the formation of the cold zone is due to the tidal bottom mixing, Fig. 10 shows distributions of temperature and vertical diffusivity in a meridional section of the channel. In the temperature distribution, the distances among the isotherms in the lower layer were wider (the stratification was weakened) in the cold zone from 32.9 to 33.3° N compared with the offshore region, and a dome structure was seen in the upper layer. This indicates that mixing was strengthened in the lower layer of the cold zone, and as a result, the cold water of the lower layer affected the upper layer. In the distribution of the vertical diffusivity, bottom mixing was actually so strong that the strong mixing region of  $10 \text{ cm}^2 \text{ s}^{-1}$  extended from the bottom to the depth of 20 m, which supports the theory (Fig. 10b). It should be noted that the strengthening of bottom mixing by tides and the change of temperature stratification were reproduced in the model by the tidal motion and the GLS turbulent mixing scheme. The Seto Inland Sea model also reproduced the tidal front, but it was necessary to use the tidal mixing parameterization to strengthen the mixing externally, since explicit tides were not introduced (Sakamoto et al. 2016).

The SST in summer is relatively low in some strait regions such as the Itsuki-Nada Strait, the Naruto Strait, and the Kii Channel, suggesting the tidal influence on SST (Fig. 9). Especially in the Osaka Bay and the Kochi Bay, SST was somewhat lower than the observation. It is considered that the tidal mixing may be excessive or temperature of river inflows may be too low, indicating that there is still room for improvement of the coastal region reproducibility. Undulation of the spring and neap tidal cycle was found in SST of the Bungo Channel as reported by Iwasaki et al. (2015) (not shown), which should be analyzed in the future.

As mentioned above, there are few systematic observational data of the internal structure in the coastal seas around Japan, but there are several research reports on thermal stratification of the Seto Inland Sea (Guo et al. 2004). Above all, Yu et al. (2016) is valuable because it reveals the seasonal development of the temperature difference between the surface layer and the bottom layer based on observation data for 30 years. In order to make a direct comparison with their results (Fig. 4), the temperature difference was similarly calculated from the 4-year model experiment results (Fig. 11). As a result, it was found that the seasonal development of temperature stratification was well reproduced by the model. In April, the temperature difference was less than 1 °C, and the winter mixed layer reached the bottom. From May, stratification began to form in the middle of relatively

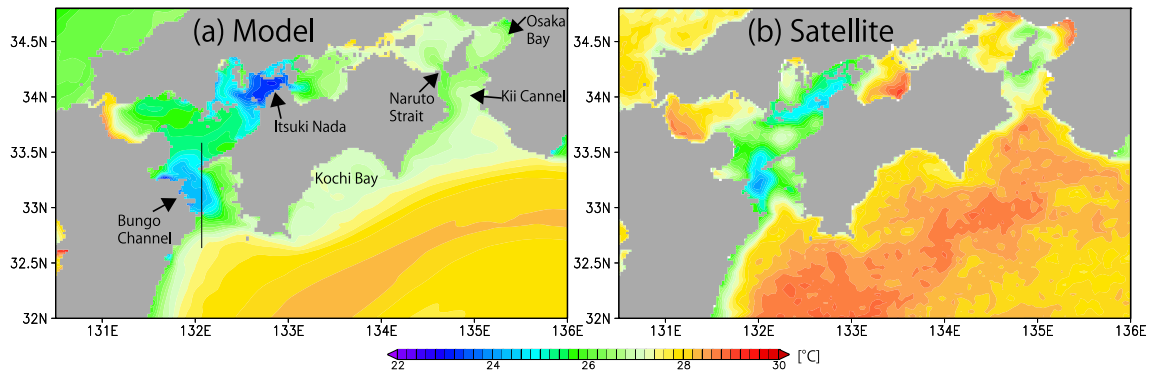


**Fig. 9** Mean SST in August 2011 for **a** the model and **b** the satellite observation. **a** The black line in the Bungo Channel is the section shown in Fig. 10

large regions, and the temperature difference increased with June and July. It peaked in August and weakened sharply in September. The amplitude of the temperature difference in summer was also consistent with Yu et al. (2016), as it reached 6 °C or more in the Bungo Channel and the Kii Channel, where the Kuroshio water flows in, and in the middle of several large regions. However, some local features were not reproduced. For example, in the Akashi Strait, the temperature difference is 8 °C or more in the model, but Yu et al. (2016) shows 2 °C or less even in summer. This is considered to be a side effect of intentionally suppressing tidal currents in this strait in order to tune the tides in the Seto Inland Sea (Section 4.2). In the Hiuchi-Nada region, the temperature difference was only 2 °C in the model, but Yu et al. (2016) shows 6 °C or more. Despite these discrepancies, the seasonal development of temperature stratification in the Seto Inland Sea was realistically reproduced as a whole. Considering that stratification could hardly be verified in the development of the Seto Inland Sea model (Sakamoto et al. 2016), this result is important.

Verification of the internal structure in other regions is a future subject, but the same degree of reproducibility as the Seto Inland Sea may be expected.

The coastal salinity field was also generally reproducible in the range of the available observational data. Figure 12 is a comparison of sea surface salinity (SSS) with an observation result. In May 2009, the model SSS tended to be a little lower, but its pattern was roughly consistent. In the western region of the Seto Inland Sea, SSS was high due to the inflow of the Kuroshio water through the Bungo Channel, as the contour line of 33 was found near 133.5° E. Also in the Kii Channel, SSS was over 33 in the east side of the channel due to the inflow of the Kuroshio water. On the other hand, SSS in the Osaka Bay was low due to the riverine fresh water inflow from the Yodo River, which is one of the largest rivers in Japan. In October, these features were the same as in May, but SSS decreased by one (Fig. 12c). This seasonal change also coincides with the observation (Fig. 12d). RMSE for the SSS observation data was 0.83 on average for 32 months for which observation

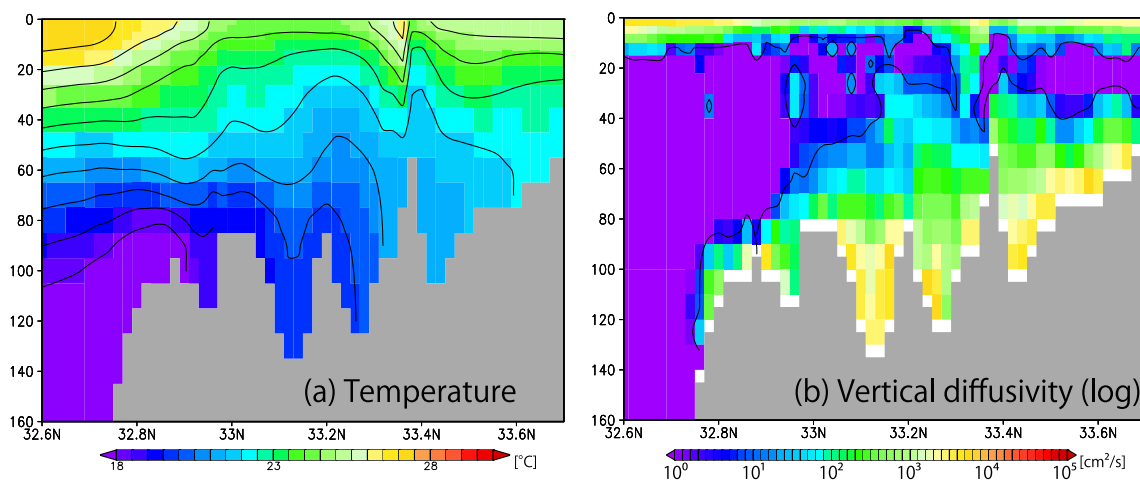


**Fig. 10** **a** Temperature and **b** vertical diffusivity in a section from the 32.6 to 33.7° N (the black line in Fig. 9). They are the mean values in August 2011. **a** The contour line interval is 1 °C. **b** Only the contour lines of 10 cm<sup>2</sup> s<sup>-1</sup> are shown

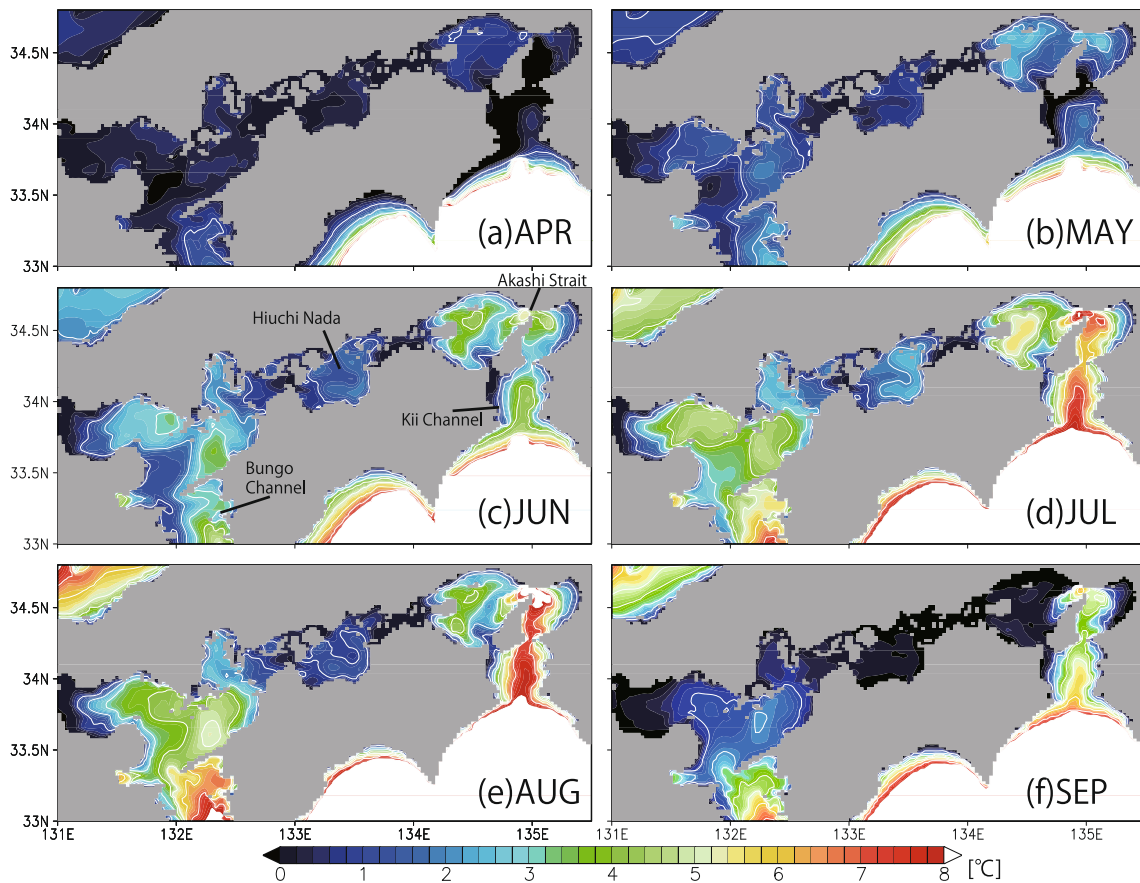


**Fig. 11** Difference in temperature ( $^{\circ}\text{C}$ ) between the model surface layer and the bottom layer in the 4-year average from (a) April to (f) September. It was constructed so that it could be compared directly

with Fig. 4 of Yu et al. (2016), including the color shade. The interval of the contour lines (white lines) is  $1^{\circ}\text{C}$

data are available in 2009–2012. (RMSE for May and October 2009 shown in Fig. 12 were nearly average values as 0.72 and 0.86, respectively.) Comparing Fig. 12 in details,

the model had lower SSS than the observation along the northern coast of the eastern region. Although there is a possibility that river runoff is excessive in the model, the

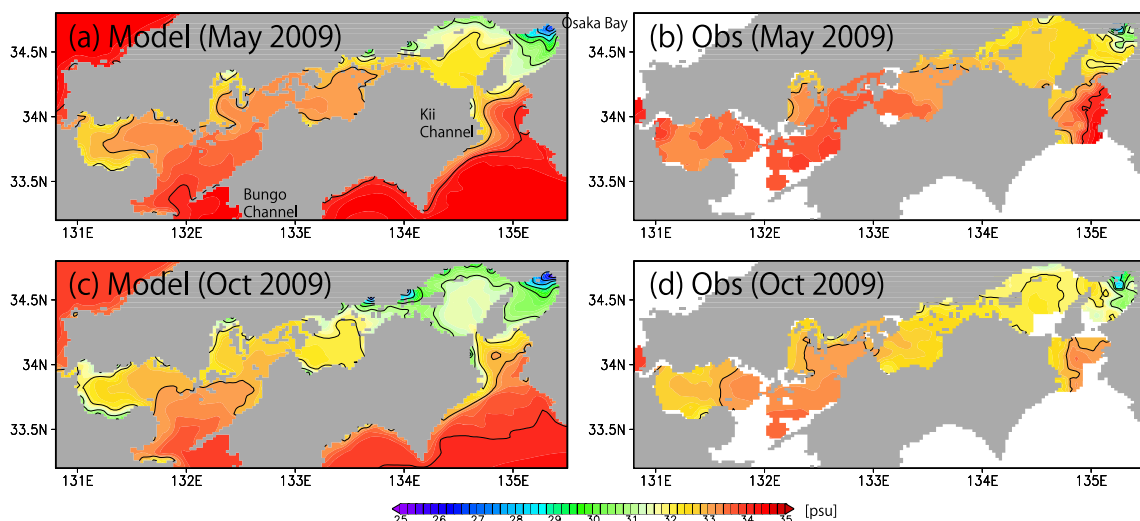


**Fig. 12** Monthly mean SSS in the Seto Inland Sea for a, c the model and b, d the observation complied by the Seto Inland Sea Comprehensive Water Quality Survey. The results of a, b May and c, d October

are shown since the observation has the largest amount of data in these months for 2009. The contour interval is  $1\text{ psu}$

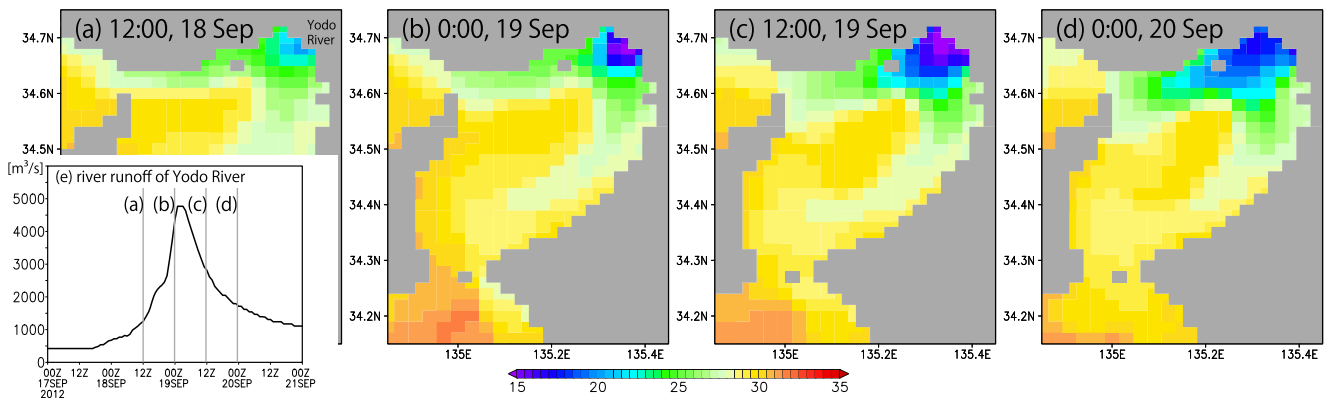


**Fig. 13** SSS variations in the Osaka Bay every 12 h from 12:00 on September 18, 2012. The time series inserted is the Yodo River inflow rate, and the four vertical lines in the figure indicate the times from **a** to **d**

observation may not have a resolution to capture the low SSS signal near the coasts. Higher resolution observational data are necessary for further verification.

In the experiment, we used the JMA runoff index dataset to give approximately 4000 river inflows across Japan with a fine temporal resolution of 1 h (Urakawa et al. 2016). The model can simulate short-term phenomena such as formation of low-salinity plumes after large flooding accompanied by a typhoon. Figure 13 shows SSS in the Osaka Bay during 2 days after passing of a typhoon. Due to the heavy rain, the Yodo River inflow into the Osaka Bay increased about 10 times as much as the normal state on September 19. As a result, a low-salinity plume below 15 was formed near the river mouth (Fig. 13b), and then a part went south on a clockwise circulation, while a part went west along the shore (Fig. 13c, d). We could not obtain SSS data in the Osaka Bay observed on such short-term scale, but we would like to examine its reproducibility and impact on the oceanic condition in future.

At the end of this section, we examine reproduction of the well-known thermohaline front of the Kii Channel in

winter. Figure 14 shows mean SST, SSS, and sea surface density in February. These distributions were similar to the observation made in the same season of 1966 (Akitomo et al. 1990). Both SST and SSS were high in the southern open ocean and low in the northern coastal sea, and therefore, strong meridional gradients were formed in the Kii Channel. On the other hand, looking at the density field, the temperature and salinity effects on density canceled each other so that it rather reached a maximum in the central part of the channel. This characteristic phenomenon, which is called the thermohaline front, has been attracting attention, and we succeeded in reproducing it in the model. This result shows that temperature and salinity in the coastal regions had some reproducibility as shown above and that, therefore, the density field related to dynamics was also well reproduced.

### 3.3 Coastal currents

Observation data of coastal currents are more sparse than temperature and salinity so that verification is more

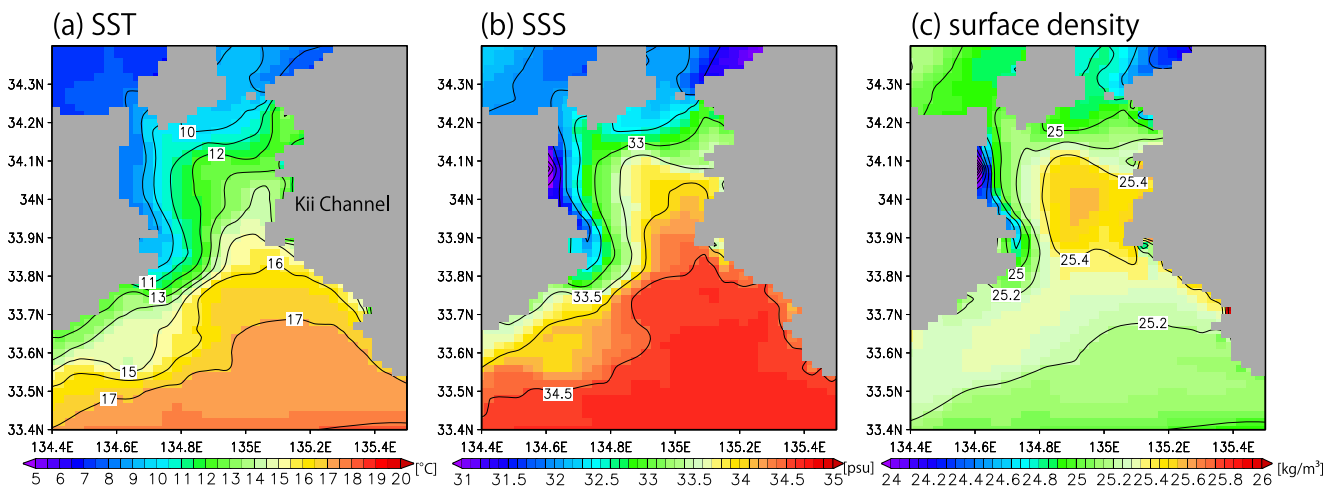


**Fig. 14** **a** SST, **b** SSS, and **c** sea surface density in the Kii Channel averaged on February 1 to 9, 2012. The contour intervals are **a** 1 °C, **b** 0.5, and **c** 0.2 kg m<sup>-3</sup>, respectively

difficult. One of the few exceptions is transport through the main three straits connected to the Sea of Japan, the Tsushima Strait, the Tsugaru Strait, and the Soya Strait (e.g. Hirose et al. 1996; Tsujino et al. 2008; Fukudome et al. 2010; Ohshima et al. 2017). Therefore, we verified the model results by comparing the seasonal variations of the transports with the multi-model ensemble results of Han et al. (2016), which is one of the latest research. Figure 15 shows the inflow transport rate through the Tsushima Strait to the Sea of Japan and the outflow transport rates through the Tsugaru Strait and the Soya Strait. The transport rate for the Tsushima Strait decreased to 2 Sv or less in winter and became up to 3 Sv in August ( $1 \text{ Sv} = 10^6 \text{ m}^3 \text{ s}^{-1}$ ). For the Tsugaru Strait, it was as small as 1.5 Sv or less in winter and increased to 2 Sv in fall. For the Soya Strait, it was almost zero in January and increased to over 1 Sv in August. These features are in good agreement with the seasonal variations shown by Han et al. (2016). The annual mean values, 2.27 Sv at the Tsushima Strait, 1.65 Sv at the Tsugaru Strait, and 0.64 Sv at the Soya Strait, are also close (85–98%) to the results of Han et al. (2016), 2.40 Sv, 1.68 Sv, and 0.72 Sv, respectively. It is suggested that basic seasonal variations of the coastal currents around Japan were reproduced by the model even without data assimilation.

## 4 Results: coastal sea level variations

In this section, we systematically verify the coastal sea level variations. The tide gauge data used has the following advantages for verification of the coastal model. First, it

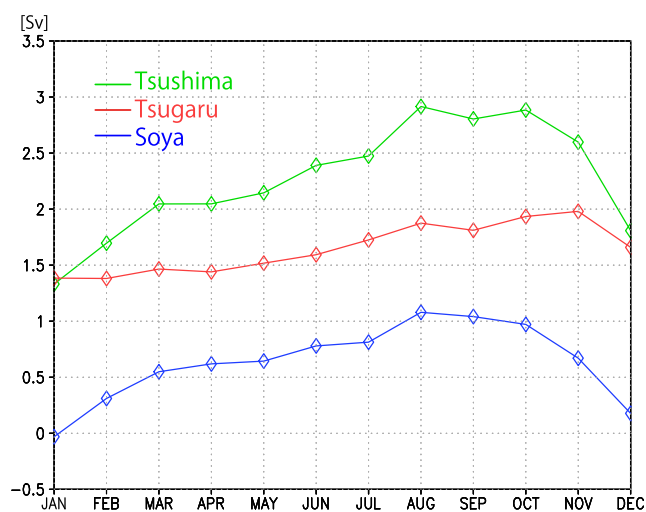


**Fig. 15** Monthly transports through the Tsushima Strait (green), the Tsugaru Strait (red), and the Soya Strait (blue). They are the experimental results averaged from 2009 to 2012, and the unit is Sv ( $= 10^6 \text{ m}^3 \text{ s}^{-1}$ ). The transport of the Tsushima Strait indicates the inflow into the Sea of Japan, while the other two show the outflow. The graph is created in accordance with Fig. 15 of Han et al. (2016)

covers the entire coast of Japan with approximately 200 sites. This is important considering that satellite data and ARGO data cannot be used enough in coastal seas and there are few observation data with wide coverage. Second, the observation has been continued for several years to decades with a fine time resolution of 1 h. We can investigate phenomena of various time scales appearing on the sea level variations. Third, one of the main operational purposes of the model is coastal disaster prevention, which is a motivation for verifying the coastal sea level. In addition to the overall reproducibility, a rapid rise event is also shown at the last subsection. (Here, the term “sea level” has the same meaning as sea surface height (SSH).)

## 4.1 Overview

An example of the sea level (SSH) field reproduced by the model is shown in Fig. 16a. Sea level change of 1 m or more accompanied by the Kuroshio current appeared south of Japan, and many cyclonic and anti-cyclonic eddies on the scale of several hundred kilometers were seen offshore. In coastal seas such as the East China Sea, the Yellow Sea, and the Seto Inland Sea, tidal elevation of 1 m or more was conspicuous. In this way, phenomena of the various spatiotemporal scales appeared in the sea level distribution.

Next, to show an overall picture of the coastal sea level variations, a power spectrum at Kobe is shown in Fig. 17 as a representative example. The amplitude of the seasonal variation with the wave number 1 was the largest as approximately 20 cm, and the amplitude tended to decrease as the wave number increased. Several spikes were found near the 1-day cycle and the half-day cycle, and they corresponded to the diurnal and semidiurnal tides given to the model, as indicated by the gray lines in the figure. These features are consistent with the observation (the black line), indicating that the variation characteristics were simulated realistically on wide time scales from several hours to 1 year. It is interesting that some peaks of periods shorter than half a day were also reproduced (the arrows in the figure). Although the model was driven by only the main 8 tidal constituents, it is suggested that overtides and compound tides were reproduced to some extent by nonlinear dynamics in the model.

## 4.2 Tides

As seen from the spectral analysis of Kobe (Fig. 17), the tides were dominant in short-term variations of several days, except for in the Sea of Japan. Figure 16 b and c show the sea level variations at Kobe and Tokyo, respectively, during 6 days around the time of Fig. 16a. The variation seemed a more sinusoidal wave at Tokyo, which is close to the Pacific Ocean, while distortion was strengthened

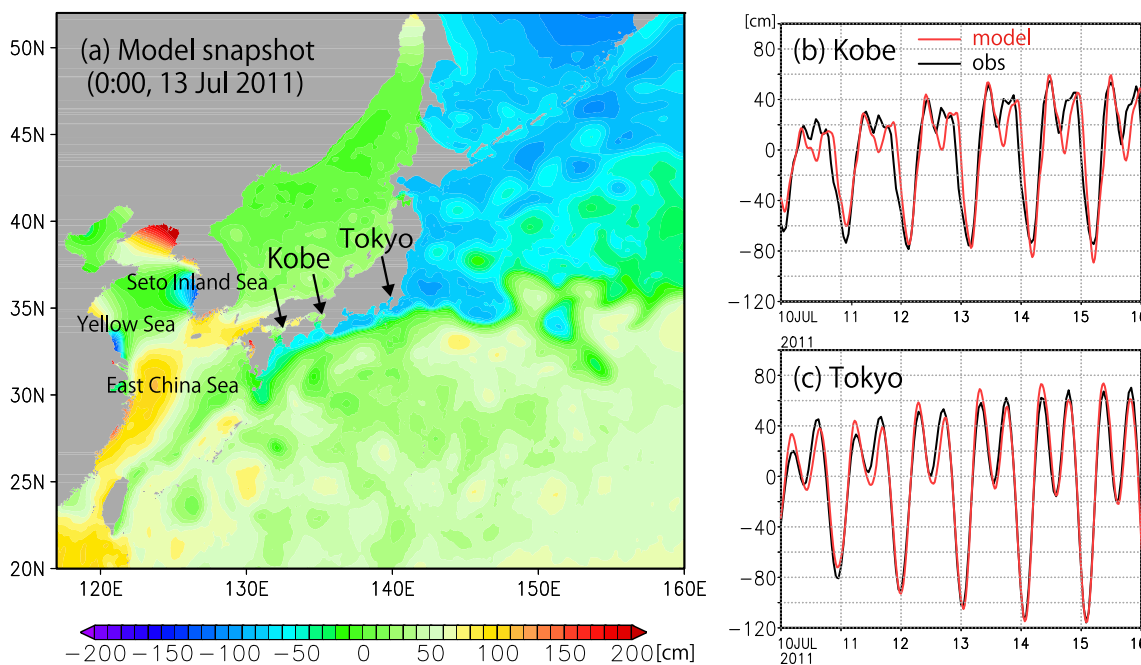


**Fig. 16** **a** Sea level at 0:00 on July 13, 2011, in the model. **b, c** Time series of sea level variations for six days from July 10, 2011, at **b** Kobe and **c** Tokyo. The red lines indicate the model results, while black lines indicate the tide gauge observation. The mean values of the display period are subtracted

by nonlinear dynamics at Kobe, which is in an inner bay of the Seto Inland Sea. Though the difference existed, tidal variations of several tens of centimeters to 1 m were commonly seen. The reproducibility was slightly lower at

Kobe, where the nonlinearity is stronger, but the model generally followed the observation well.

In order to examine the tidal reproducibility systematically, we conducted a harmonic analysis with the periods of the main 8 tidal constituents. Because the results were similar for any constituent, the result for the M2 tide of the largest amplitude is shown in Fig. 18. The M2 tidal amplitude was as large as 30–60 cm on the Pacific coast of Japan, 90–150 cm in the East China Sea, and up to 100 cm in the Seto Inland Sea, whereas it was as small as 10 cm or less in the Sea of Japan. Such distribution corresponds well to the tide gauges indicated by the circles in the figure and also tide analysis data such as FES2014 (not shown). The Greenwich phase increased from north to south along the Pacific coast, and from the East China Sea to the Sea of Japan, indicating the progress of tidal waves. A change in the phase was also seen in the Seto Inland Sea, indicating that it progressed from the open ocean to the inner regions. Although the wave progression was shifted in some coastal areas such as around the Hokkaido Island and in the Osaka Bay (the maximum error was 69° at Himeji), the Greenwich phase was also roughly consistent with the observation. The error of the M2 tidal amplitude with respect to the tide gauge data was 4.0 cm on average, corresponding to 9.2% of the amplitude itself, and the phase error was 10.2°. For example, the errors for the assimilated tidal model with horizontal resolution of 1/2° of Matsumoto et al. (2000) are 8.3 cm and 14.4°, respectively. Thus, we could incorporate tides to the model with good accuracy, in spite of using only theoretical

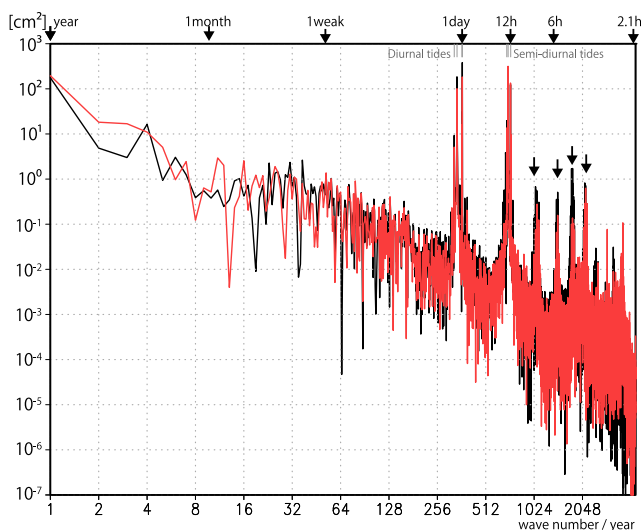


**Fig. 17** Power spectrum of the sea level variations at Kobe in 2009. Both the horizontal axis and the vertical axis are represented by logarithm, and the wave number 1 of the seasonal variation and the wave number 4096 of the 2.14-h cycle are shown. The red line indicates the model, while the black line indicates the observation. The short gray lines at the top of the figure show the frequencies of the diurnal and semidiurnal tides given to the model. The arrows indicate peaks considered to be overtides or compound tides. See Fig. 16a for the location of Kobe

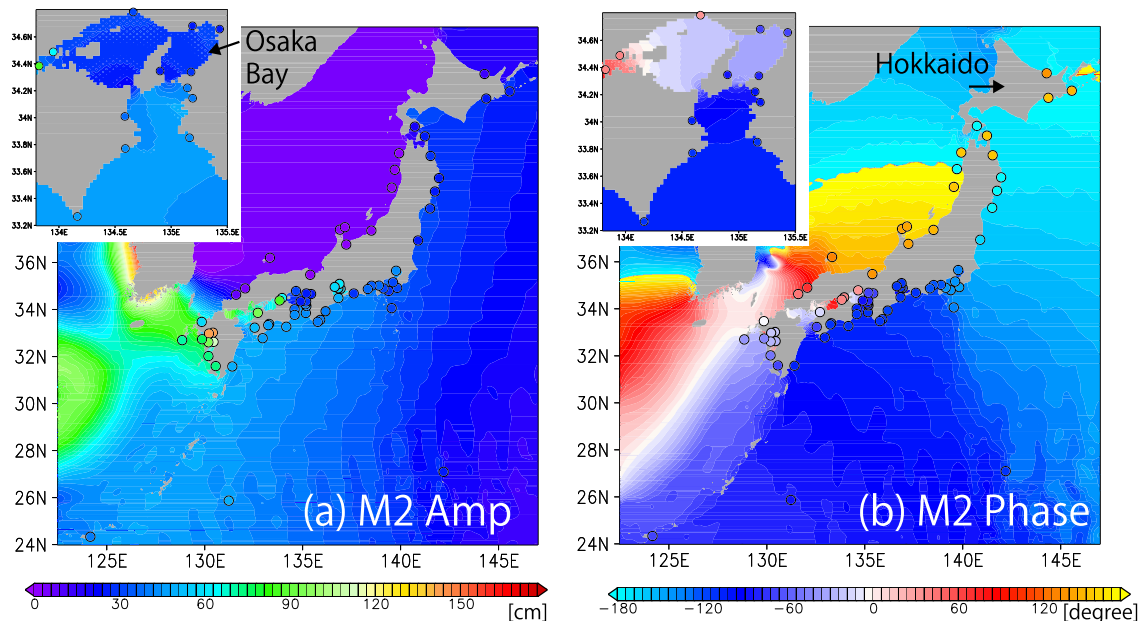


**Fig. 18** **a** The amplitude and **b** the Greenwich phase of the M2 tide obtained by harmonic analysis of the sea level variations. The circles indicate the results of the tide gauges. The figures inserted in the upper left are enlarged views of the eastern Seto Inland Sea

tidal potentials without any observation data. This is due to our tide scheme (Sakamoto et al. 2013) as explained in Section 2.1. (For the Japanese coastal tide model with horizontal resolution of  $1/12^\circ$  of Matsumoto et al. (2000), the errors are small as  $2.5\text{ cm}$  and  $3.2^\circ$ , respectively. However, it is not a fair comparison since the tide gauge data itself is used for its data assimilation.)

### 4.3 Daily mean time series

Next, in order to verify the sea level variations on longer time scales, a time series of the daily mean is shown in Fig. 19 for 1 year. As in many areas of the coasts of

Japan, the model sea level followed the observation well at Kobe. The seasonal variation of up to  $50\text{ cm}$ , where it was low in winter and high in summer, was reproduced well. Sudden rises due to typhoon passages in the middle of July and early September were simulated by incorporating the inverse barometer effect into the model. However, there were also drifts over several weeks during the period from May to October. Since the drifts were corrected in the data assimilation experiment (the blue line in the figure, see Hirose et al. (2019) for the data assimilation experiment), stochastic fluctuations of large-scale phenomena in open oceans, such as mesoscale eddies or the Kuroshio path variation, are considered to be the cause. The largest gap

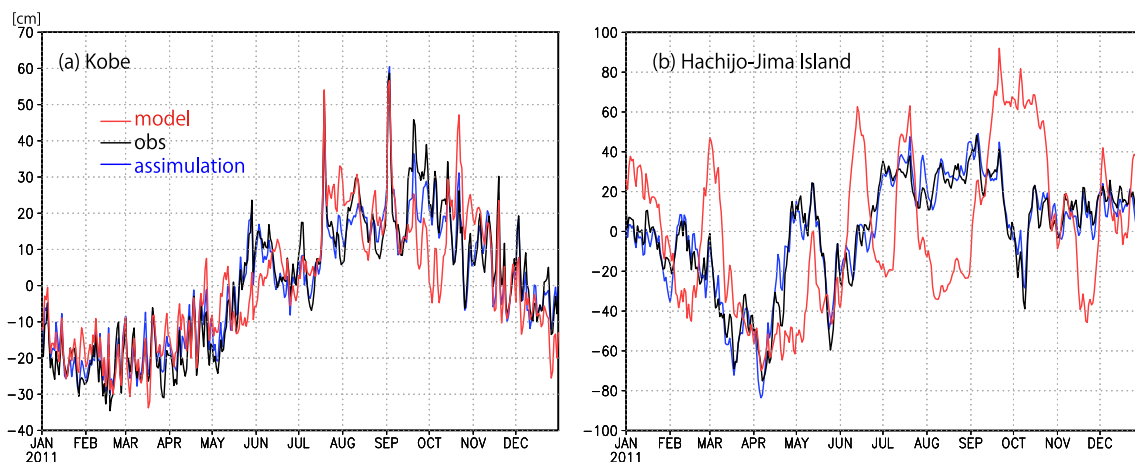


**Fig. 19** Time series of the daily mean sea level in 2011 at **a** Kobe and **b** the Hachijo-Jima Island. The red lines indicate the model results, black lines indicate the tide gauge observation, and blue lines indicate

the data assimilation experiment results. The mean value of the displayed period is subtracted in each. The locations of Kobe and the Hachijo-Jima Island are indicated in Fig. 20



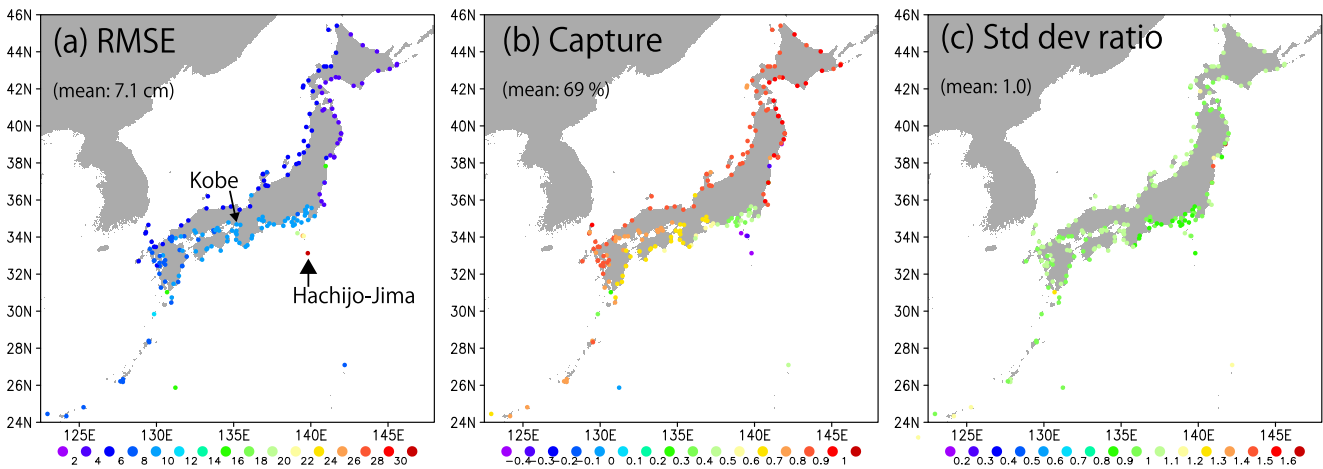


**Fig. 20** **a** The RMSE, **b** the capture ratio  $C$ , and **c** the standard deviation ratio  $R$  of the model daily mean sea level against the tide gauge observation. They were evaluated in the whole experimental period from 2009 to 2012. See the text for the calculation formula, Eq. 3

appeared at the Hachijo-Jima Island, which locates in the Kuroshio current region (Fig. 19b). Sea level variations up to 1 m are observed on time scales from several weeks to several months. In the model, the sea level fluctuated with similar time scales and amplitudes, but the phase did not match so that the error was over 50 cm. Although this error cannot be avoided in free-run experiments, it can be corrected by data assimilation (blue line).

In order to systematically show the reproducibility of the daily mean sea level  $\eta$  against the tide gauge observation  $\eta_o$  throughout the coasts of Japan, the root mean square error RMSE, the capture ratio  $C$ , and the standard deviation ratio  $R$  are calculated as follows:

$$\begin{aligned}
 \text{RMSE} &= \left\{ \overline{(\eta' - \eta_o')^2} \right\}^{1/2} \\
 C &= 1 - \frac{\overline{(\eta' - \eta_o')^2}}{\overline{\eta_o'^2}} \\
 R &= \left\{ \frac{\overline{\eta'^2}}{\overline{\eta_o'^2}} \right\}^{1/2}, \tag{3}
 \end{aligned}$$

where

$$\eta' = \eta - \bar{\eta}, \quad \eta_o' = \eta_o - \bar{\eta}_o, \tag{4}$$

and the overbars indicate the 4-year mean. From the three indicators shown in Fig. 20, the sea level reproducibility on the coast of Japan can be roughly divided into three regions: the southern coast of Japan affected by the Kuroshio current, the Seto Inland Sea, and others (Table 2). On the southern coast of Japan, the indicators were relatively bad: RMSE was up to 8–12 cm and  $C$  was only 30–60%. Since  $R$  was as small as 70–90 %, the sea level variations accompanied by the Kuroshio current fluctuation may be underestimated in the model. As shown in Fig. 19b, RMSE reached a maximum of 39.4 cm on Hachijo-Jima, which is directly affected by the Kuroshio. In the Seto Inland Sea, the

indicators were better, as RMSE was 8–10 cm,  $C \sim 70\%$ ,  $R$  90–110%. This improvement may be because the coastal sea level in the Seto Inland Sea is less affected by the Kuroshio current fluctuation. On other coasts, RMSE was as small as 6 cm or less,  $C$  reached over 80%, and  $R$  close to 100%. It shows that the sea level variations were reproduced well. In the overall mean values, RMSE was 7.1 cm, the capture ratio  $C$  was 69%, and  $R$  was 101%. Since there has not been such a systematic model verification targeting the coastal seas of Japan as far as we know, they cannot be compared with past research. However, these indicators show good reproducibility of the model as a whole, considering that no data assimilation is used. Initialization by data assimilation further improved RMSE to 4.4 cm and  $C$  to 89% ( $R$  remained almost 100%).

#### 4.4 A rapid rise event

At the end of this section, we show an example of reproducing an event where a rapid sea level rise occurred, regarding coastal disaster prevention. In this event, the sea level rose

**Table 2** The RMSE, the capture ratio  $C$ , and the standard deviation ratio  $R$  in three representative regions around Japan and their average values over the entire regions. The values are summarized based on the maps of Fig. 20. The average values of the assimilation experiment are also added as a reference

Region	RMSE	$C$ (%)	$R$ (%)
Southern coasts of Japan (130–140° E)	8–12 cm	30–60	70–90
Seto Inland Sea	8–10 cm	~ 70	90–110
Other coasts	< 6 cm	> 80	90–110
Mean	7.1 cm	69	101
Mean (assimilation)	4.4 cm	89	102

by more than 50 cm on the Japanese coast of the Sea of Japan on September 17–18, 2012, after Typhoon Sanba passed northwards over the East China Sea. Some flooding damages were also reported (Weather Fast Report at the Maizuru Marine Meteorological Observatory, September 21, 2012). We examine how the model reproduced the sea level rise.

Figure 21 shows the time evolution of the detided sea level,  $\eta_{\text{detide}}$ , for 2 days in the relevant area. Here,  $\eta_{\text{detide}}$  refers to the deviation from the tidal variation obtained by harmonic analysis. Immediately after passing of the typhoon,  $\eta_{\text{detide}}$  rose in the northern part of the East China Sea due to the inverse barometer effect (Fig. 21a). After that, a part of the rise moved eastward along the Japanese coast and merged with a rise caused by the Ekman flow accompanied by eastward wind, resulting in a sharp rise in the coastal area (Fig. 21b). Then, the rise moved eastward as a coastal wave (Fig. 21c) and reached the Wakasa Bay while attenuating the amplitude (Fig. 21d, e). This is how the high sea level was excited and propagated in the model. The phase velocity of continental shelf waves in this area is reported as  $3\text{--}4\text{ m s}^{-1}$  (Isozaki 1968). Since the propagation speed of the rise in the model is estimated to be approximately  $3.9\text{ m s}^{-1}$  (it propagated 500 km in 1.5 days as indicated in Fig. 21b, e), the propagation of a continental shelf wave was considered to be simulated by the model.

The time series of  $\eta_{\text{detide}}$  is shown in Fig. 22 at Hamada and Maizuru. In the tide gauge observation at Hamada, a rise of approximately 55 cm occurred at 19:00 on September 17. At Maizuru, which locates downstream of the wave propagation,  $\eta_{\text{detide}}$  rose by approximately 50 cm at 13:00 on September 18. In the model, the rise of the same degree occurred at the same time, although it was slightly smaller as approximately 50 cm at Hamada and 40 cm at Maizuru. This result shows that the excitation and propagation of the continental shelf wave in the model was realistic. This is an encouraging result towards the use of this model for coastal disaster prevention.

Two additional experiments were conducted to find out what specifications of the model contributed to the good reproducibility. The case LowResForce is an experiment in which the forcings of wind and atmospheric pressure were changed from the MSM dataset of 5-km horizontal resolution to the JRA55-do dataset of 55-km resolution. In this case, the initial excitation was weak as the sea level rise became small at Hamada (Fig. 22a). It is thought that the inverse barometer effect and the Ekman flow during passing of the typhoon became small due to the smoothed forcings. Another case is OfflineSLP where the inverse barometer effect was added to  $\eta_{\text{detide}}$  later, instead of being explicitly

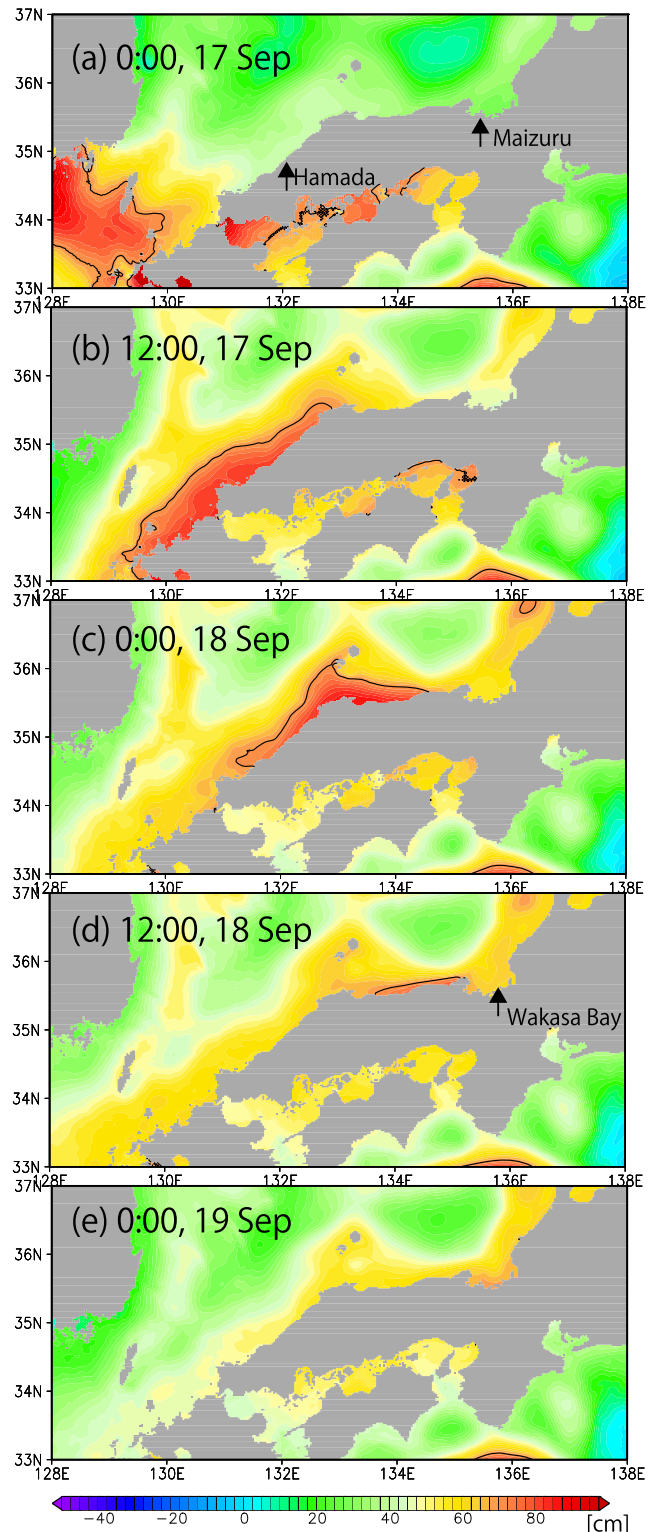


**Fig. 21** The detided sea level,  $\eta_{\text{detide}}$ , every 12 h from 0:00 on September 17, 2012, to 0:00 on 19, where  $\eta_{\text{detide}}$  is the sea level minus the tidal variation obtained by harmonic analysis of the main 8 tidal constituents. The black lines indicate contour lines of 70 cm

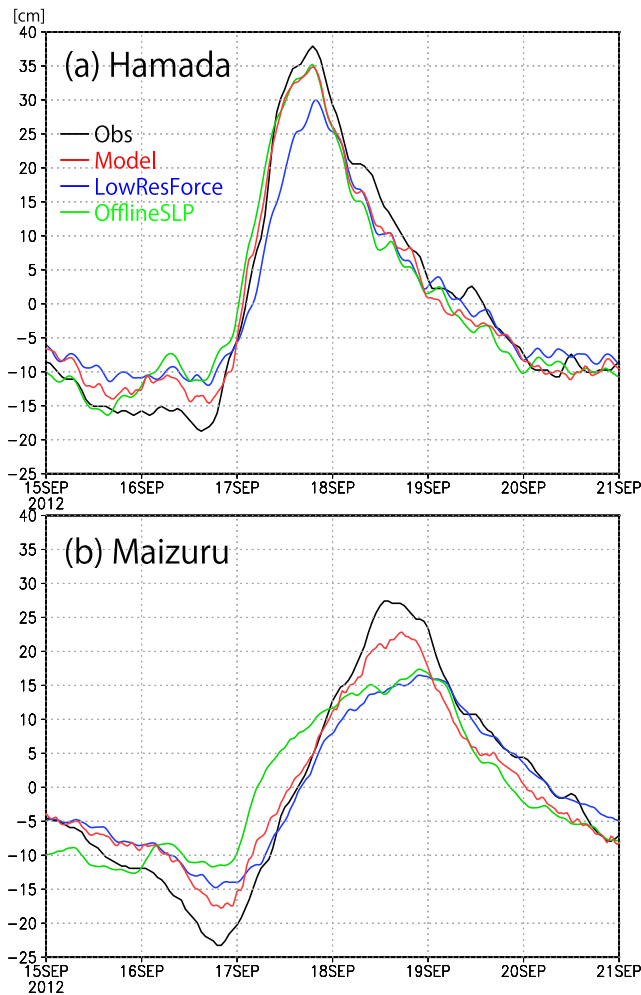


**Fig. 22** Time series of the detided sea level,  $\eta_{detide}$ , from September 15 to 21, 2012 at **a** Hamada and **b** Maizuru. The black lines are the tide gauge observation, while red lines are the model results. In addition, the blue lines are the result of the case (LowResForce) where the atmospheric forcings are changed to a low-resolution dataset, while green lines are the result of the case (OfflineSLP) where the inverse barometer effect is added to  $\eta_{detide}$  later, instead of being explicitly incorporated into the model. The locations of Hamada and Maizuru are shown in Fig. 21a. A running average of 3 h is applied

incorporated into the model. In this case, the initial rise was reproduced well, but the downstream rise became small such as at Maizuru (Fig. 22b). This is probably because the process by which the sea level rise formed by the inverse barometer effect propagates as a continental shelf wave was not reproduced. Although this is only one case, the results suggest that the use of high-resolution atmospheric forcings and the explicit introduction of the inverse barometer effect are important for simulating coastal sea level rises.

In Section 4, by comparison with the tide gauge observation, we showed that the coastal sea level variations

in the model were realistic in a wide range of time scale from tides, rapid rises in several days to the seasonal variation. Although it is verification of the sea level variations at the limited sites, it is shown that various coastal ocean processes were realistically simulated by the model.

## 5 Conclusions

In order to expand the coastal ocean monitoring and forecasting system of the Japan Meteorological Agency from the Seto Inland Sea to the entire coastal seas of Japan, a 2-km resolution model has been newly developed. This model is a two-way double-nested model based on MRI.COM Ver.4.5, coupling a global model, a North Pacific model, and a Japanese coastal model. In order to simulate various coastal phenomena around Japan for an operational use, it has been advanced from the current Seto Inland Sea model (Sakamoto et al. 2016) in many respects. We investigate its overall performance from various viewpoints, based on a 4-year hindcast experiment driven by atmospheric reanalysis data. In the experiment, initialization by data assimilation was not done to focus on the performance of the model itself.

The main results of the verification about ocean conditions are as follows:

- Regarding physical quantities such as sea surface temperature (SST), sea level, eddy kinetic energy of the sea surface geostrophic currents, basic distributions, and seasonal variations were simulated realistically. The root mean square error against monthly mean satellite SST data was 1.31 °C on average, which was reduced by 38% from a previous high-resolution Japanese coastal model (2.10 °C) (Sakamoto et al. 2010). By coupling a 5-category sea ice model, a good reproduction was shown about the sea ice development in the Sea of Okhotsk during winter. Preservation of the seawater volume was realized by coupling of the global model by the two-way nesting scheme (Section 3.1).
- The well-represented SST distributions observed characteristics in coastal seas, such as south of the Hokkaido Island and the Seto Inland Sea. Due to the high resolution, representation of coastal fronts with sharp and fine structures improved. In the Seto Inland Sea, the seasonal development of temperature stratification could be also verified as well as SST. The coastal salinity field was also generally reproducible partly because of introduction of river runoff. (The root mean square error against surface salinity observation data in the

Seto Inland Sea was 0.83 on average.) By using a high-resolution JMA river data, development of low-salinity plumes after large flooding was simulated. Thus, both temperature and salinity fields in coastal seas were well simulated, and this may be the reason why the complex thermohaline front in the Kii Channel during winter was reproduced (Section 3.2).

- As a validation of coastal currents, the transport rates through the three channels connecting to the Sea of Japan were compared with the latest research. Though slightly smaller, the model time mean transport rates match well as 95% for the Tsushima Strait, 98% for the Tsugaru Strait, and 85% for the Soya Strait. Their seasonal variations were also consistent (Section 3.3).

Verification of coastal sea level variations also gave good results:

- By using our own scheme (Sakamoto et al. 2013), we could incorporate explicit tides with high accuracy. The sea level variations of the model well followed the tide gauge observation not only at coasts facing open oceans but also in inland seas. A systematic verification by harmonic analysis showed good results such as 9.2% for the M2 amplitude error and 10.2° for the M2 phase error. It was also suggested that tidal mixing simulated in the model contributed to reproduction of the tidal front in the Bungo Channel (Sections 4.1 and 4.2).
- Characteristics of the sea level variations were realistic even on time scales longer than tides. The time series of the daily mean sea level closely followed the tide gauge observation, and its root mean square error (RMSE) was 7.1 cm and the capture ratio was 69%, which are good reproducibility scores. However, on the southern coasts of Japan affected by the Kuroshio current, the model variance of the sea level variations tended to be small as 70–90%, and the RMSE was relatively large as 8–12 cm (Section 4.3).
- Some cases of rapid sea level rise were successfully reproduced. For example, after a typhoon passed over the East China Sea on September 16, 2012, a rapid rise of 50 cm or more occurred along the west coast of the Honshu Island and propagated from west to east. The timing and the amplitude of the rise were in good agreement with the observation. This reproduction was contributed by use of high-resolution atmospheric forcings and introduction of the inverse barometer effect (Section 4.4).

As described above, the experimental results were verified from a wide range of viewpoints including temperature, salinity, currents, and sea level variations. The system using this model is expected to be widely used for

coastal disaster prevention and ocean condition monitoring, and our results support the utility of the system.

On the other hand, some problems were found in the model verification. First, in inland seas such as the Seto Inland Sea, there were errors in the tides, as an error of 69° was seen in the M2 phase at maximum. Since the spatial resolution is insufficient to simulate fully tidal currents in narrow strait regions, there is a possibility that the friction caused by the coastal topographies could not be accurately represented. Improvement of the resolution is difficult due to numerical costs, but it could be improved by optimizing the friction using a Green function method as done in the coastal model of Kyushu University (Hirose et al. 2007). In addition, SST in summer tended to be lower by 2 °C than the satellite observation in some coastal seas of strong tides, such as the Seto Inland Sea. In this model, we introduced the GLS turbulent mixing scheme, which has the potential to reproduce the bottom boundary mixing, but its verification and tuning are a future task. Furthermore, the verification in the paper is limited to physical quantities at the sea surface, except for temperature stratification in the Seto Inland Sea and the transport rates through the three straits. For example, considering that temperature in the sub-surface layer of the Sea of Japan tended to be warm in the model (not shown), it is necessary to verify the stratification. However, observational data is too sparse for such 3D validation, and it is essential to enhance the coastal observation network. In this respect, observations by submerged gliders seem prospective, which have been started at the Meteorological Research Institute and the Japan Sea National Fisheries Research Institute.

We have also developed a new data assimilation system for the operational use of the model. As shown in Fig. 19, offshore stochastic phenomena, such as the path change of the Kuroshio current and generation of mesoscale eddies, can be modified by initialization using the data assimilation, in order for the results to be compared directly to observation. As an example of the results, the error in the daily mean sea level variations (Eq. 3) decreased from 7.1 to 4.4 cm. See Usui et al. (2015) and Hirose et al. (2019) for details of the new data assimilation system. Currently, JMA is developing an operational system based on the model and the data assimilation system, and the operation is planned to be started in 2020.

**Acknowledgments** We thank the members of the oceanography and geochemistry research department of Meteorological Research Institute and the global environment and marine department of Japan Meteorological Agency for fruitful discussions and helpful comments. MODIS data is provided by the Japan Aerospace Exploration Agency/National Aeronautics and Space Administration.

**Funding information** This research was supported in part by JSPS KAKENHI Grant Number 16H02226, joint research of the Research Institute for Applied Mechanics, Kyushu University (RIAM), and

“the Social Implementation Program on Climate Change Adaptation Technology (SI-CAT)” of the Ministry of Education, Culture, Sports, Science and Technology (MEXT), Japan.

## References

- Akitomo K, Imasato N, Awaji T (1990) A numerical study of a shallow sea front generated by buoyancy flux: generation mechanism. *J Phys Oceanogr* 20:172–189. [https://doi.org/10.1175/1520-0485\(1990\)020<0172:ANSOAS>2.0.CO;2](https://doi.org/10.1175/1520-0485(1990)020<0172:ANSOAS>2.0.CO;2)
- Arakawa A (1972) Design of the ucla general circulation model. numerical simulation of weather and climate. Tech Rep. 7, Dept of Meteorology, University of California, Los Angeles
- Debreu L, Blayo E (2008) Two-way embedding algorithms: a review submitted to ocean dynamics: special issue on multi-scale modelling: nested grid and unstructured mesh approaches. *Ocean Dyn* 58(5–6):415–428. <https://doi.org/10.1007/s10236-008-0150-9>
- Debreu L, Marchesiello P, Penven P, Cambon G (2012) Two-way nesting in split-explicit ocean models: algorithms, implementation and validation. *Ocean Modell*: 49–50:1–21
- Fujisaki A, Yamaguchi H, Duan F, Sagawa G (2007) Improvement of short-term sea ice forecast in the southern okhotsk sea. *J Oceanogr* 63(5):775–790. <https://doi.org/10.1007/s10872-007-0066-x>
- Fujisaki A, Yamaguchi H, Duan F, Sagawa G (2010) Numerical experiments of air–ice drag coefficient and its impact on ice–ocean coupled system in the sea of okhotsk. *Ocean Dyn* 60(2):377–394. <https://doi.org/10.1007/s10236-010-0265-7>
- Fukudome KI, Yoon JH, Ostrovskii A, Takikawa T, Han IS (2010) Seasonal volume transport variation in the Tsushima Warm Current through the Tsushima Straits from 10 years of ADCP observations. *J Oceanogr* 66(4):539–551
- Griffies SM, Hallberg RW (2000) Biharmonic friction with a Smagorinsky-like viscosity for use in large-scale eddy-permitting ocean models. *Mon Wea Rev* 128:2935–2946. [https://doi.org/10.1175/1520-0493\(2000\)128<2935:BFWASL>2.0.CO;2](https://doi.org/10.1175/1520-0493(2000)128<2935:BFWASL>2.0.CO;2)
- Guo X, Futamura A, Takeoka H (2004) Residual currents in a semi-enclosed bay of the seto inland sea, Japan. *J Geophys Res* 109:C12,008. <https://doi.org/10.1029/2003JC002203>
- Han S, Hirose N, Usui N, Miyazawa Y (2016) Multi-model ensemble estimation of volume transport through the straits of the East/Japan sea. *Ocean Dyn* 66(1):59–76. <https://doi.org/10.1007/s10236-015-0896-9>
- Hirose N, Kim CH, Yoon JH (1996) Heat budget in the Japan sea. *J Oceanogr* 52(5):553–574
- Hirose N, Kawamura H, Lee HJ, Yoon JH (2007) Sequential forecasting of the surface and subsurface conditions in the Japan sea. *J Oceanogr* 63(3):467–481
- Hirose N, Usui N, Sakamoto K, Tsujino H, Yamanaka G, Nakano H, Urakawa S, Toyoda T, Fujii Y, Kohno N (2019) Development of a new operational system for monitoring and forecasting coastal and open ocean states around Japan (in preparation)
- Hunke EC, Dukowicz JK (1997) An elastic-viscous-plastic model for sea ice dynamics. *J Phys Oceanogr* 27:1849–1867. [https://doi.org/10.1175/1520-0485\(1997\)027<1849:AEVPMF>2.0.CO;2](https://doi.org/10.1175/1520-0485(1997)027<1849:AEVPMF>2.0.CO;2)
- Hunke EC, Dukowicz JK (2002) The elastic-viscous-plastic sea ice dynamics model in general orthogonal curvilinear coordinates on a sphere: incorporation of metric terms. *Mon Wea Rev* 130:1848–1865. [https://doi.org/10.1175/1520-0493\(2002\)130<1848:TEVPSI>2.0.CO;2](https://doi.org/10.1175/1520-0493(2002)130<1848:TEVPSI>2.0.CO;2)
- Ishizaki H, Yamanaka G (2010) Impact of explicit sun altitude in solar radiation on an ocean model simulation. *Ocean Modell* 33:52–69. <https://doi.org/10.1016/j.ocemod.2009.12.002>
- Isozaki I (1968) An investigation on the variations of sea level due to meteorological disturbances on the coast of Japanese islands (ii) storms surges on the coast of the Japan sea. *J Oceanogr Soc Jpn* 24(4):178–190
- Iwasaki S, Isobe A, Miyao Y (2015) Fortnightly atmospheric tides forced by spring and neap tides in coastal waters. *Sci Rep* 5:10,167. <https://doi.org/10.1038/srep10167>
- Kuroda H, Setou T, Kakehi S, ichi Ito S, Taneda T, Azumaya T, Inagake D, Hiroe Y, Morinaga K, Okazaki M, Yokota T, Okunishi T, Aoki K, Shimizu Y, Hasegawa D, Watanabe T (2017) Recent advances in Japanese fisheries science in the kuroshio-oyashio region through development of the fra-roms ocean forecast system: overview of the reproducibility of reanalysis products. *Open J Marine Sci* 7:62–90. <https://doi.org/10.4236/ojms.2017.71006>
- Large WG, Yeager SG (2004) Diurnal to decadal global forcing for coean and sea-ice models: the data sets and flux climatologies. NCAR Tech. Note: TN-460+STR, CGD Division of the Natinal Center for Atmospheric Research
- Matsumoto K, Takanezawa T, Ooe N (2000) Ocean tide models developed by assimilating TOPEX/POSEIDON altimeter data into hydrodynamical model: a global model and a regional model around Japan. *J Oceanogr* 56:567–581. <https://doi.org/10.1023/A:1011157212596>
- Mellor GL, Kantha L (1989) An ice-ocean coupled model. *J Geophys Res* 94:10,937–10,954. <https://doi.org/10.1029/JC094iC08p10937>
- Merryfield WJ, Holloway G (2003) Application of an accurate advection algorithm to sea-ice modelling. *Ocean Modell* 5(1):1–15. [https://doi.org/10.1016/S1463-5003\(02\)00011-2](https://doi.org/10.1016/S1463-5003(02)00011-2)
- Mey PD, Stanev E, Kourafalou VH (2017) Science in support of coastal ocean forecasting -part 1. *Ocean Dyn* 67(5):665–668. <https://doi.org/10.1007/s10236-017-1048-1>
- Miyazawa Y, Varlamov SM, Miyama T, Guo X, Hihara T, Kiyomatsu K, Kachi M, Kurihara Y, Murakami H (2017) Assimilation of high-resolution sea surface temperature data into an operational nowcast/forecast system around Japan using a multi-scale three-dimensional variational scheme. *Ocean Dyn* 67(6):713–728. <https://doi.org/10.1007/s10236-017-1056-1>
- Nakano H, Tsujino H, Sakamoto K (2013) Tracer transport in cold-core rings pinched-off from the kuroshio extension in an eddy-resolving ocean general circulation model. *J Geophys Res* pp –, <https://doi.org/10.1002/jgrc.20375>
- Noh Y, Kim HJ (1999) Simulations of temperature and turbulence structure of the oceanic boundary layer with the improved near-surface process. *J Geophys Res* 104:15
- Ohshima KI, Simizu D, Ebuchi N, Morishima S, Kashiwase H (2017) Volume, heat, and salt transports through the soya strait and their seasonal and interannual variations. *J Phys Oceanogr* 47(5):999–1019. <https://doi.org/10.1175/JPO-D-16-0210.1>
- Prather MJ (1986) Numerical advection by conservation of second-order moments. *J Geophys Res* 91(D6):6671–6681. <https://doi.org/10.1029/JD091iD06p06671>
- Renault L, Marchesiello P, Masson S, McWilliams JC (2019a) Remarkable control of western boundary currents by eddy killing, a mechanical air-sea coupling process. *Geophys Res Lett* 46(5):2743–2751. <https://doi.org/10.1029/2018GL081211>
- Renault L, Masson S, Oerder V, Jullien S, Colas F (2019b) Disentangling the mesoscale ocean-atmosphere interactions. *J Geophys Res Oceans* 124(3):2164–2178. <https://doi.org/10.1029/2018JC014628>
- Sakamoto K, Tsujino H, Nishikawa S, Nakano H, Motoi T (2010) Dynamics of the Coastal Oyashio and its seasonal variation in a high-resolution western North Pacific Ocean model. *J Phys Oceanogr* 40(6):1283–1301. <https://doi.org/10.1175/2010JPO4307.1>

- Sakamoto K, Tsujino H, Nakano H, Hirabara M, Yamanaka G (2013) A practical scheme to introduce explicit tidal forcing into an OGCM. *Ocean Sci* 9:1089–1108. <https://doi.org/10.5194/os-9-1089-2013>
- Sakamoto K, Yamanaka G, Tsujino H, Nakano H, Urakawa S, Usui N, Hirabara M, Ogawa K (2016) Development of an operational coastal model of the seto inland sea, Japan. *Ocean Dyn* 66(1):77–97. <https://doi.org/10.1007/s10236-015-0908-9>
- Senjyu T, Enomoto H, Matsuno T, Matsui S (2006) Interannual salinity variations in the tsushima strait and its relation to the changjiang discharge. *J Oceanogr* 62(5):681–692. <https://doi.org/10.1007/s10872-006-0086-y>
- Simpson JH, Hunter JR (1974) Fronts in the irish sea. *Nature* 250:404–406. <https://doi.org/10.1038/250404a0>
- Tsujino H, Nakano H, Motoi T (2008) Mechanism of currents through the straits of the Japan sea: mean state and seasonal variation. *J Oceanogr* 64:141–161
- Tsujino H, Nakano H, Sakamoto K, Urakawa S, Hirabara M, Ishizaki H, Yamanaka G (2017) Reference manual for the Meteorological Research Institute Community Ocean Model version 4 (MRI.COMv4). Tech Rep 80, Meteorological Research Institute, Japan. <https://doi.org/10.11483/mritechrepo/80>
- Tsujino H, Urakawa S, Nakano H, Small RJ, Kim WM, Yeager SG, Danabasoglu G, Suzuki T, Bamber JL, Bentsen M, Böning CW, Bozec A, Chassignet EP, Curchitser E, Dias FB, Durack PJ, Griffies SM, Harada Y, Ilicak M, Josey SA, Kobayashi C, Kobayashi S, Komuro Y, Large WG, Sommer JL, Marsland SJ, Masina S, Scheinert M, Tomita H, Valdivieso M, Yamazaki D (2018) JRA-55 Based surface dataset for driving ocean-sea-ice models (JRA55-do). *Ocean Modell* 130:79–139. <https://doi.org/10.1016/j.ocemod.2018.07.002>
- Uchiyama Y, Suzue Y, Yamazaki H (2017) Eddy-driven nutrient transport and associated upper-ocean primary production along the Kuroshio. *J Geophys Res Oceans* 122(6):5046–5062. <https://doi.org/10.1002/2017JC012847>
- Umlauf L, Burchard H (2003) A generic length-scale equation for geophysical turbulence models. *J Marine Res* 61(2):235–265. <https://doi.org/10.1357/002224003322005087>
- Urakawa LS, Kurogi M, Yoshimura K, Hasumi H (2015) Modeling low salinity waters along the coast around Japan using a high resolution river discharge data set. *J Oceanogr* 71(6):715–739. <https://doi.org/10.1007/s10872-015-0314-4>
- Urakawa LS, Tsujino H, Nakano H, Sakamoto K, Yamanaka G, Toyoda T (2019) Weakening of the bottom cell of meridional overturning circulation by spurious diapycnal mixing caused by practical implementations of the isopycnal tracer diffusion scheme (in preparation)
- Urakawa S, Yamanaka G, Hirabara M, Sakamoto K, Tsujino H, Nakano H (2016) Assessment of the usefulness of jma runoff index in coastal ocean modeling around Japan. *Weather Service Bulletin* 83:S33–S45. (in Japanese)
- Usui N, Fujii Y, Sakamoto K, Kamachi M (2015) Development of a four-dimensional variational assimilation system toward coastal data assimilation around Japan. *Mon Weather Rev* 143:3874–3892. <https://doi.org/10.1175/MWR-D-14-00326.1>
- Usui N, Wakamatsu T, Tanaka Y, Hirose N, Toyoda T, Nishikawa S, Fujii Y, Takatsuki Y, Igarashi H, Nishikawa H, Ishikawa Y, Kuragano T, Kamachi M (2017) Four-dimensional variational ocean reanalysis: a 30-year high-resolution dataset in the western north pacific (fora-wnp30). *J Oceanogr* 73:205–233. <https://doi.org/10.1007/s10872-016-0398-5>
- Varlamov SM, Guo X, Miyama T, Ichikawa K, Waseda T, Miyazawa Y (2015) M2 baroclinic tide variability modulated by the ocean circulation South of Japan. *J Geophys Res Oceans* 120(5):3681–3710. <https://doi.org/10.1002/2015JC010739>
- Watanabe T, Ikeda M, Wakatsuchi M (2004) Thermohaline effects of the seasonal sea ice cover in the sea of okhotsk. *J Geophys Res* 109(C9):C09S02. <https://doi.org/10.1029/2003JC001905>
- Yanagi T, Koike T (1987) Seasonal variation in thermohaline and tidal fronts, Seto Inland Sea, Japan. *Continental Shelf Res* 7(2):149–160. [https://doi.org/10.1016/0278-4343\(87\)90076-8](https://doi.org/10.1016/0278-4343(87)90076-8)
- Yoshimura H, Yukimoto S (2008) Development of a simple coupler (scup) for earth system modeling. *Pap Meteorol Geophys* 59:19–29. <https://doi.org/10.2467/mripapers.59.19>
- Yu X, Guo X, Takeoka H (2016) Fortnightly variation in the bottom thermal front and associated circulation in a semienclosed sea. *J Phys Oceanogr* 46:159–177. <https://doi.org/10.1175/JPO-D-15-0071.1>
- Yukimoto S, Kawai H, Koshiro T, Oshima N, Yoshida K, Urakawa S, Tsujino H, Deushi M, Tanaka T, Hosaka M, Yabu S, Yoshimura H, Shindo E, Mizuta R, Obata A, Adachi Y, Ishii M (2019) The mri earth system model version 2.0, mri-esm2.0: description and basic evaluation of the physical component (submitted to *Journal of the Meteorological Society of Japan*)